Lawrence Berkeley National Laboratory

Title
NUMERICAL STUDY OF INCOMPRESSIBLE SLIGHTLY VISCOUS FLOW PAST BLUNT BODIES AND AIRFOILS

Permalink
https://escholarship.org/uc/item/71b294sh

Author
Cheer, Angela Yit Lear

Publication Date
1981-05-01

Lawrence Berkeley Laboratory
UNIVERSITY OF CALIFORNIA

Physics, Computer Science & Mathematics Division

NUMERICAL STUDY OF INCOMPRESSIBLE SLIGHTLY VISCOUS
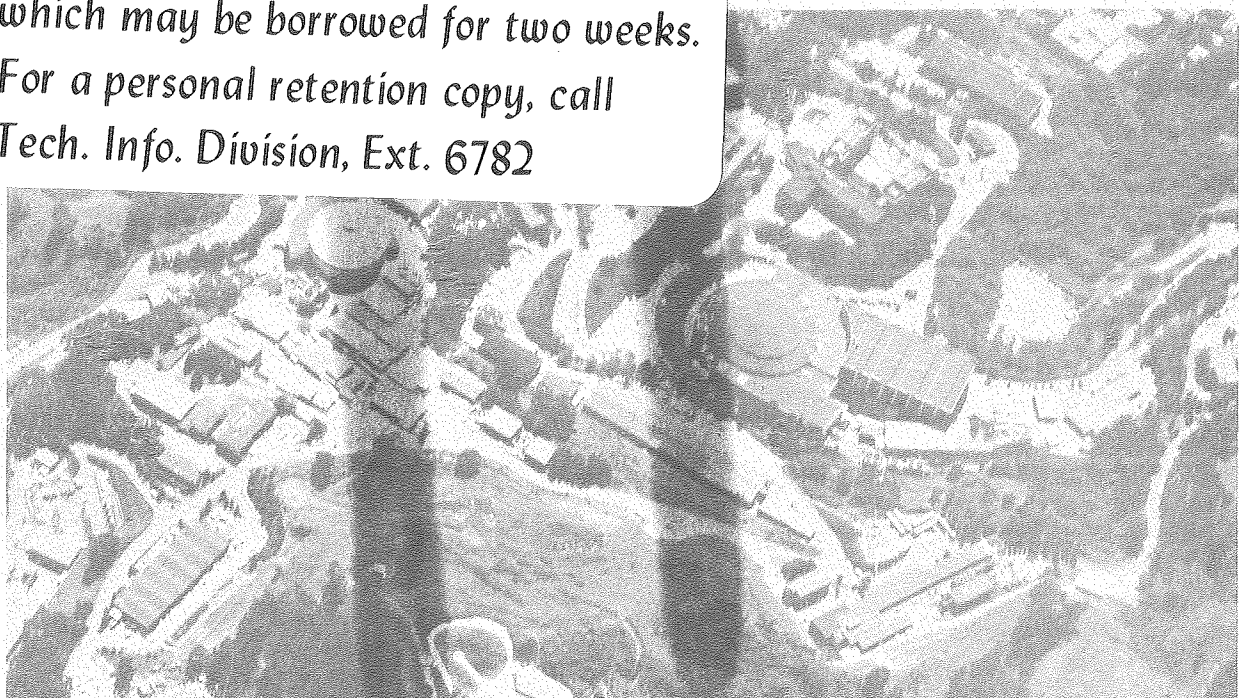FLOW PAST BLUNT BODIES AND AIRFOILS

Angela Yit Lean Cheer
(Ph.D. thesis)

May 1981

DISCLAIMER

NUMERICAL STUDY OF INCOMPRESSIBLE SLIGHTLY VISCOUS

FLOW PAST BLUNT BODIES AND AIRFOILS

Angela Yit Lean Cheer

Ph.D. Thesis

May 1981

Lawrence Berkeley Laboratory
University of California
Department of Mathematics
Berkeley, California 94720

To the CHEERs and to the memory
of my Grandmother, K. S. Fong Cheer

TABLE OF CONTENTS

Numerical Study of Incompressible Slightly Viscous
Flow Past Blunt Bodies and Airfoils

Angela Yit Lean Cheer

Lawrence Berkeley Laboratory
University of California
Department of Mathematics
Berkeley, California 94720

ABSTRACT

A grid free numerical method is used to simulate incompressible flow at high Reynolds number. The numerical method simulates the flow inside the boundary layer by vortex sheets and the flow outside this layer by vortex blobs. The algorithm produces a smooth transition between the sheets and the blobs.

The accuracy of this hybrid numerical method is tested in several numerical experiments. In the first experiment, the algorithm is used to simulate slightly viscous flow past a circular cylinder. In the second experiment, the algorithm is used to simulate flow past a Joukowski airfoil at various angles of attack. In the latter case, there is no evidence of "blow-up" of the flow at the trailing edge of the airfoil. In both experiments, the calculated flow and its functionals (such as lift and drag coefficients) are in good agreement with both theoretical results and wind tunnel experiments.

1. Introduction

Viscous fluid flows can be described by the Navier-Stokes equations (see [3], [17], [25], [35], [41], [45], [46], [48], or [54]). These equations are difficult to solve numerically, especially at large Reynolds numbers. For example, a method based on a grid has the disadvantage that the mesh width must decrease as the Reynolds number R increases. Consequently, at very large Reynolds numbers, a very fine grid must be imposed or else the numerical viscosity due to the grid will swamp the effects of the true viscosity as represented by the Reynolds number. In this paper we obtain numerical solutions to the problems of flow past obstacles by using a grid-free numerical method. We apply this method to simulate flow past a circular cylinder and flow past airfoils at varying angles of attack.

Consider a steady two-dimensional flow of a fluid of small viscosity past a flat plate with no slip at the solid surface. If we neglect viscosity and thus calculate the flow as a potential flow without discontinuities, then it is impossible to satisfy the no-slip condition at the boundary. However, the no-slip condition can be satisfied by assuming that a vortex sheet coincides with the solid surface. The relative tangential velocity then falls to zero through that sheet. As the fluid of small viscosity passes the obstacle, the vorticity created at the boundary diffuses, and then this vorticity is convected downstream. The diffusion distance in the normal direction is small, and the main effect of convection carries the vorticity parallel to rather than away from the body. The result is to produce a layer of

large vorticity adjacent to the solid surface. Through this layer the tangential velocity falls from its value in the main stream to zero at the surface. Suppose the flow past the flat plate has velocity $\underline{U} = (1,0)$ parallel to the stream. The time required for the fluid of viscosity ν to traverse a unit distance along the x-direction of the plate is of order x/U. In this time the vorticity attains a finite but appreciable value within a layer whose thickness is of the order $(\nu x/U)^{1/2} = (1/R)^{1/2}$. This is the order of the thickness of the boundary layer. See [50] for a history of boundary layer theory and [55] for a discussion of incompressible boundary layer separation.

A similar analysis can be applied to the motion of the flat plate started impulsively from rest. Initially, the flow is irrotational and without circulation. The initial impulse produces a vortex sheet coincident with the solid surface. This vorticity immediately begins to diffuse, and is eventually convected downstream. After a short time t there is a boundary layer whose thickness is of order $(\nu t)^{1/2}$. Thus, in the case of flow past an obstacle and in the case of flow due to the motion of an obstacle started impulsively from rest, we see that there are two regions to consider, namely, the flow in the regions inside and outside the boundary layer. In our study, we consider the flow in these two regions separately, and then patch the two solutions together at the edge of the boundary layer.

In this paper, flow past an obstacle started impulsively from rest will be simulated by a hybrid numerical method. This hybrid algorithm is a coupling of the random vortex sheets and the random vortex blobs method.

The random vortex blobs methods was first presented by Chorin in 1973 [9]. This is a grid free numerical method where the inviscid part of the equations is studied through interactions of vortex blobs; the effects of viscosity are studied through use of the relationship between diffusion and random walks; and the no-slip condition is satisfied via a vorticity generation algorithm. An outline of this method is presented in Section 2. There are, however, some difficulties with this method. First, the convergence near the boundary is slow, and second the interaction between blobs is singular. The random vortex sheets method was presented by Chorin in 1978 [10]. Vortex sheet elements can be used near the boundary to solve the Prandtl boundary layer equations. This method is also grid-free and has the advantage that the interaction between vortex sheet elements are not singular. A more detailed discussion can be found in Section 4.

The hybrid algorithm introduced in this paper consists of the following: The flow inside the boundary layer is approximated by the vortex sheet method. The flow outside the boundary layer is approximated by the vortex blobs method. These two methods are coupled at the edge of the boundary layer. In this coupling, we replace the vortex blobs with vortex sheets near the boundary thereby eliminating the problem of convergence of the vortex blobs near the boundary of the obstacle. The interaction between the blobs and sheets is not singular, and thus this new method poses no additional complications. Section 5 gives a more detailed description of how the coupling is done to produce this hybrid method.

To test the accuracy of this hybrid algorithm, we applied it to several problems. The first application was to the problem of flow past a circular cylinder. The second application was to the problem of flow past an airfoil at varying angles of attack. The numerical results, as presented in Sections 8 and 10 indicate that we have a good model for simulating viscous fluid flow in two-dimensions. For both cases, the results of the numerical calculations are in good agreement with results obtained from physical experiments. For our hybrid method, new computational elements are introduced when we satisfy the boundary conditions, and the total number of computations at each time step is of order $O(n^2)$, where n is the total number of computational elements.

2. Random Vortex Blobs Method in Two Dimensions

The Navier-Stokes equations for an incompressible flow can be written as:

$$(1) \qquad \xi_t + (\underline{U} \cdot \underline{\nabla}) \xi = R^{-1} \Delta \xi$$

$$(2) \qquad \Delta \psi = -\xi$$

$$(3) \qquad u = \psi_y \quad , \quad v = -\psi_x$$

where $\underline{U} = (u,v)$ is the velocity field, $\xi = \text{curl } \underline{U}$ is the vorticity, t represents the time, ψ is the stream function, $\Delta = \nabla^2$ is the Laplace operator, $z = (x,y)$ is the position vector, and R is the Reynolds number.

Let us first consider the above system of three equations in a region without boundaries. Solving the Poisson Equation (2) above, we obtain the solution:

$$(4) \qquad \psi(x,y) = \iint E(x-\bar{x}, y-\bar{y})(-\xi(\bar{x},\bar{y})) d\bar{x} d\bar{y}$$

where $E(x,y) = (1/2\pi) \log((x^2 + y^2)^{1/2})$ is the fundamental solution of the Laplace equation. If $\xi = \xi(\underline{r})$ is radially symmetric, then $\psi = \psi(\underline{r})$ and $\nabla \xi = \lambda(x,y)\nabla \psi$. Thus, $(\underline{U} \cdot \underline{\nabla}) \xi = 0$, and equation (1) above reduces to the diffusion equation

$$(5) \qquad \xi_t = R^{-1} \Delta \xi \quad .$$

The system of equations (3), (4) and (5) lends itself well to the following numerical scheme. First, we solve (2) analytically to

obtain $\psi(x,y)$. Then $\psi(x,y)$ can be approximated using "essentially" the discrete form of equation (4). Second, we find $\underline{U} = (u,v)$ by taking the derivatives of $\psi(x,y)$ according to equations (3). Finally, we give each element a random walk, where the method of random walks is used to approximate the diffusion equation (5) above. We now summarize the details of this numerical scheme.

Consider a point vortex of strength k_0 located at some point $z_0 = (x_0, y_0)$. The corresponding stream function is

$$(6) \qquad \psi(z) = k_0 \cdot (2\pi)^{-1} \log|z - z_0| \qquad ,$$

where $|z - z_0|$ is the distance between the points z and z_0. From the relationship (3) we can easily find the induced velocity by taking the derivatives of the stream function. Thus,

$$(7) \qquad \begin{aligned} u(x,y) &= \frac{-1}{2\pi} k_0 \left(\frac{y - y_0}{r_0^2} \right) \\[2em] v(x,y) &= + \frac{1}{2\pi} k_0 \left(\frac{x - x_0}{r_0^2} \right) \end{aligned}$$

where $r_0^2 = (x - x_0)^2 + (y - y_0)^2$. Hence, the trajectory of the vortex is described by $dx/dt = u$ and $dy/dt = v$.

We start by taking the initial distribution of vorticity say $\xi(0)$, and partition it into a finite number of sections. Each section has vorticity distribution ξ_j, $j = 1, 2, \ldots, N$. We visualize our computational elements as point vorticies situated at points $z_j = (x_j, y_j)$

with strength k_j where $k_j = \int \xi_j \, dxdy$ is the circulation. Initially at time $t = 0$, we consider the flow corresponding to $\xi(o) = \sum_{j}^{N} k_j \cdot \delta(z-z_j)$, where δ is the delta function. From (6) we see that the corresponding stream functions are given by

$$\psi = \sum_{j=1}^{N} \psi_j$$

where

$$\psi_i = (2\pi)^{-1} \sum_{\substack{j=1 \\ j \neq i}}^{N} k_j \, \log|z_i - z_j| \qquad i = 1, 2, \ldots, N$$

with

$$\Delta\psi_j = -\xi_j \qquad .$$

From (3) and (7) we obtain the velocity of the vortex point situated at z_i;

$$
\begin{aligned}
u_i &= -(2\pi)^{-1} \sum_{j} k_j \left(\frac{y_i - y_j}{r_{ij}^2} \right) \\
(8) \\
v_i &= (2\pi)^{-1} \sum_{j} k_j \left(\frac{x_i - x_j}{r_{ij}^2} \right) \qquad \text{,}
\end{aligned}
$$

where r_{ij} is the distance between the points (x_i, y_i) and (x_j, y_j).

Let us now consider the structure of a point vortex. Let $\underline{r}$ be any radius vector joining the center of the vortex to some point of the fluid. The induced velocity at a point of distance r away from the vortex has magnitude inversely proportional to r and direction perpendicular to $\underline{r}$. Thus, the induced velocity tends to zero at great

distances. However, as $\underline{r}$ tend to zero, the induced velocity tends to infinity, which is physically unrealistic. These characteristics can be verified from equations (8) with $r_{ij} \to 0$. As discussed in Chorin [9], what we need is a smoother stream function $\psi^0(r)$ such that

$$\psi = \sum_{j=1}^{N} k_j \psi^0(z-z_j)$$

where

$$\psi^0 \begin{cases} \cong (2\pi)^{-1} \log r & r \text{ large} \\ \\ \to 0 & \text{as } r \to 0 \end{cases}.$$

In this way, we also revise the motion of the vortices to get

$$(9) \quad \begin{aligned} \frac{dx_i}{dt} &= - \sum_{j \neq i} k_j \partial_y \psi^0 \\ \frac{dy_i}{dt} &= \sum_{j \neq i} k_j \partial_x \psi^0 \end{aligned},$$

Revising the stream function in this way has the effect of changing the computational elements from vortex points into vortex blobs. Each blob has small compact support. The circulation $k_j = \int \xi_j\, dxdy$ is now integrated over the support of the blob situated at point z_j. For this study we use the following revised stream function:

$$(10) \quad \psi^0(r) = \begin{cases} (2\pi)^{-1} \log r & r \geqq \sigma \\ (2\pi)^{-1} r/\sigma & r < \sigma \end{cases}$$

where r denotes the distance and σ is a cut-off length to be determined later. For more information on cut-offs, including comparative studies and convergence proofs, see Hald [19] and Hald and DelPrete [21]. The induced velocities using this new stream function are:

$$
\begin{aligned}
-u_i &= (2\pi)^{-1} \sum_{r_{ij}>\sigma} k_j \left(\frac{y_i-y_j}{r_{ij}^2}\right) + (2\pi)^{-1} \sum_{r_{ij}\leq\sigma} k_j \left(\frac{y_i-y_j}{\sigma r_{ij}}\right) \\
v_i &= (2\pi)^{-1} \sum_{r_{ij}>\sigma} k_j \left(\frac{x_i-x_j}{r_{ij}^2}\right) + (2\pi)^{-1} \sum_{r_{ij}\leq\sigma} k_j \left(\frac{x_i-x_j}{\sigma r_{ij}}\right) \quad .
\end{aligned}
$$

(11)

Next, we consider the diffusion part of the Navier-Stokes equation,
$$\xi_t = R^{-1}\Delta\xi, \quad \xi = \xi(x,y,t)$$

with initial condition $\xi(x,y,t=0) = \xi(0)$. Here we use random walks to simulate the diffusion process as follows: First, distribute over the plane point masses ξ_i located at $z_i = (x_i,y_i)$ with the condition that $\sum_i \xi_i = \xi(0)$. Next, move the points according to the laws

$$
X_i^{n+1} = X_i^n + n_1 \quad , \qquad Y_i^{n+1} = Y_i^n + n_2 \quad ,
$$

where n_1 and n_2 are independent random variables with a gaussian distribution of mean zero and variance $2 \cdot \Delta t/R$, where Δt represents the time step and (x_i^n, y_i^n) represents the ith-point at time $t=n \cdot \Delta t$. For more discussion on random walks, see references [8], [14], and [22].

Let u_i^n and v_i^n satisfy equations (11) or equivalently the right-hand side of (9), i.e., u and v are velocity components induced by the stream function (10). Then, combining the motion due to the induced velocity and random walk we arrive at the following:

(12)
$$X_i^{n+1} = X_i^n + \Delta t \ u_i^n + \eta_1$$
$$Y_i^{n+1} + Y_i^n + \Delta t \ v_i^n + \eta_2 \quad .$$

The vorticity density generated by the motion of the vortices according to these laws will approximate the solution to our system of equations (1), (2), and (3). Convergence proofs for closely related methods are presented by Beale and Majda [4], and Hald [20].

Next, let us place an obstacle in the fluid. For example, a circular cylinder or an airfoil. The boundary conditions we need to satisfy are

(13)
$$\underline{U} \cdot \underline{\tau} = 0 \qquad \text{on the boundary } \partial D, \ \underline{\tau} \text{ tangent to } \partial D$$

$$\underline{U} \cdot \underline{n} = 0 \qquad \text{on } \partial D, \text{ where } \underline{n} \text{ is normal to } \partial D.$$

To satisfy the first boundary condition, a vorticity generation algorithm will be used. The no-slip condition and the viscosity will create a boundary layer next to the obstacle. The vortex sheet method, which will be introduced later, will be used to approximate the Boundary Layer Equations and, at the same time, will take care of the induced tangential boundary condition.

For the case of a circular cylinder, the second boundary condition can be easily satisfied using the method of images. In the case of an airfoil, or an obstacle of arbitrary geometry, the boundary condition is satisfied by adding to our solution the solution of the Laplace equation with Neumann boundary condition. These procedures are described in the following section.

3. Potential Component of the Flow

We place an obstacle into a field of flow and consider the normal velocity induced on the boundary of the object. To satisfy the normal boundary condition, $\underline{u} \cdot \underline{n} = 0$ on ∂D, we need to add to the solution of our problem a potential flow with the opposite normal velocity on the boundary.

For the case of flow past a circular cylinder, this is particularly simple since we can use the method of images. Consider a vortex k situated at a point z_1 in the xy-plane, and also situated outside a circular cylinder of radius a, centered at the origin. The image system consists of a vortex $-k$ at the inverse point $1/\bar{z}_1$ and a vortex k at the origin. The vortex k at z_1 together with its inverse vortex $-k$ at $1/\bar{z}_1$ cancels exactly on the boundary, thus giving zero normal velocity. The vortex k at the origin does not influence the normal velocity on the boundary but is needed to satisfy conservation of circulation (see Figure 1).

FiGURE 1

Circle Theorem

Let there be irrotational two-dimensional flow of an incompressible inviscid fluid in the z-plane. Let there be no rigid boundaries, and let the complex potential of the flow be $f(z)$ where the singularities of $f(z)$ are all at a distance greater than a from the origin. If a circular cylinder $|z| = a$ is introduced into the field of flow, the complex potential becomes $w = f(z) + \bar{f}(a^2/z)$, where $\bar{f}$ denotes the complex conjugate of f. For proof, see Milne-Thomson [36] and [37].

To illustrate this theorem, let us take two vortices: one vortex k at point z_1 and the other vortex $-k$ at point $\bar{z}_1$ outside the cylinder of radius a centered at the origin. The complex potential in the absence of the cylinder is $ik\{\log (z-z_1)/(z-\bar{z}_1)\}$. If we insert the cylinder, we get (from the circle theorem) the complex potential

$$(14) \qquad W = ik \, \log \frac{(z-z_1)}{(z-\bar{z}_1)} - ik \, \log \left(\frac{\frac{a^2}{z} - \bar{z}_1}{\frac{a^2}{z} - z_1} \right) \qquad .$$

If we write $W_{z_1} = \phi_{z_1} + i\psi_{z_1}$ where ϕ_{z_1} is the velocity potential at point z_1 and ψ_{z_1} the stream function at point z_1, we can readily verify that the velocity vector of the vortex at z_1 is

$$\frac{1}{2} \left(-\frac{\partial \psi_{z_1}}{\partial y_1} \quad , \quad \frac{\partial \psi_{z_1}}{\partial x_1} \right) \qquad .$$

When we compare this velocity vector to equations (3), we note that we have an extra factor of 1/2 here. This is because a vortex and its inverse together influence the velocity at any one point by a factor of two. Hence, the correct velocity is one half the velocity induced by the image system as indicated by the formula above.

For flow past an airfoil, we have two cases.

Case 1: If the airfoil can be obtained easily from a conformal transformation of a circle, we make use of a theorem due to Routh.

Theorem: Under a conformal transformation

$$\widetilde{z} = f(z) \quad , \quad \widetilde{z} = \widetilde{x} + i\widetilde{y} \quad , \quad z = x + iy \quad ,$$

which derives the motion in the $\widetilde{z}$-plane from that in the z-plane, the Kirchhoff-Routh function for the new motion is given by

$$(15) \qquad \widetilde{W}_{z_1} = W_{z_1} + \frac{k}{2} \log \left| \frac{dz}{d\widetilde{z}} \right|_{z_1} \quad ,$$

where $\left| \dfrac{dz}{d\widetilde{z}} \right|_{z_1}$ is the absolute value of the derivative at point z_1. Thus, the new complex potential $\widetilde{W}_{z_1}$ is simply the old complex potential W_{z_1} plus $\frac{k}{2} \log \left| \dfrac{dz}{d\widetilde{z}} \right|_{z_1}$. For a proof of this theorem see C.C. Lin [28].

Case 2: If the airfoil, or the obstacle, is of arbitrary shape, we do the following: First, from the vortex method described in the previous section, we can find the induced velocity $\underline{U}_\xi$ at each point on the boundary of the object. Let $\underline{n} = (n_1, n_2)$ be the outward normal

Circle Theorem

Let there be irrotational two-dimensional flow of an incompressible inviscid fluid in the z-plane. Let there be no rigid boundaries, and let the complex potential of the flow be f(z) where the singularities of f(z) are all at a distance greater than a from the origin. If a circular cylinder $|z|$ = a is introduced into the field of flow, the complex potential becomes w = f(z) + $\bar{f}(a^2/z)$, where $\bar{f}$ denotes the complex conjugate of f. For proof, see Milne-Thomson [36] and [37].

To illustrate this theorem, let us take two vortices: one vortex k at point z_1 and the other vortex –k at point $\bar{z}_1$ outside the cylinder of radius a centered at the origin. The complex potential in the absence of the cylinder is $ik\{\log\ (z-z_1)/(z-\bar{z}_1)\}$. If we insert the cylinder, we get (from the circle theorem) the complex potential

$$(14) \qquad W = ik\ \log\ \frac{(z-z_1)}{(z-\bar{z}_1)} - ik\ \log\left(\frac{\dfrac{a^2}{z} - \bar{z}_1}{\dfrac{a^2}{z} - z_1}\right) \ .$$

If we write $W_{z_1} = \phi_{z_1} + i\psi_{z_1}$ where ϕ_{z_1} is the velocity potential at point z_1 and ψ_{z_1} the stream function at point z_1, we can readily verify that the velocity vector of the vortex at z_1 is

$$\frac{1}{2}\ \left(-\frac{\partial\psi_{z_1}}{\partial y_1}\ ,\ \frac{\partial\psi_{z_1}}{\partial x_1}\right) \qquad .$$

When we compare this velocity vector to equations (3), we note that we have an extra factor of 1/2 here. This is because a vortex and its inverse together influence the velocity at any one point by a factor of two. Hence, the correct velocity is one half the velocity induced by the image system as indicated by the formula above.

For flow past an airfoil, we have two cases.

Case 1: If the airfoil can be obtained easily from a conformal transformation of a circle, we make use of a theorem due to Routh.

Theorem: Under a conformal transformation

$$\tilde{z} = f(z) \quad , \quad \tilde{z} = \tilde{x} + i\tilde{y} \quad , \quad z = x + iy \quad ,$$

which derives the motion in the $\tilde{z}$-plane from that in the z-plane, the Kirchhoff-Routh function for the new motion is given by

$$(15) \qquad \tilde{W}_{z_1} = W_{z_1} + \frac{k}{2} \log \left| \frac{dz}{d\tilde{z}} \right|_{z_1} \quad ,$$

where $\left| \dfrac{dz}{d\tilde{z}} \right|_{z_1}$ is the absolute value of the derivative at point z_1.
Thus, the new complex potential $\tilde{W}_{z_1}$ is simply the old complex potential W_{z_1} plus $\frac{k}{2}\log \left| \dfrac{dz}{d\tilde{z}} \right|_{z_1}$. For a proof of this theorem see C.C. Lin [28].

Case 2: If the airfoil, or the obstacle, is of arbitrary shape, we do the following: First, from the vortex method described in the previous section, we can find the induced velocity $\underline{U}_\xi$ at each point on the boundary of the object. Let $\underline{n} = (n_1, n_2)$ be the outward normal

to the boundary. Next we find a potential flow $\underline{U}_p$ such that

$\underline{U}_p \cdot \underline{n} = -\underline{U}_\xi \cdot \underline{n}$ on the boundary. In references [13] and [53], a

numerical method for doing this is presented. Adding this potential

flow to our solution will give us a solution with a zero normal

boundary condition.

4. Vortex Sheet Method for Solving Boundary Layer Equations in Two Dimensions, and Vorticity Generation Algorithm

Let us consider the flat plate problem in the z-plane. Assume the wall to be at $y=0$ and the flow field to be in the half space $y \geq 0$. The boundary layer equations are

(16) $\quad \xi_t + (\underline{U} \cdot \underline{\nabla}) \xi = \nu \xi_{yy}$,

(17) $\quad \xi = -u_y$,

(18) $\quad u_x + v_y = 0$,

with the following boundary conditions,

(19) $\quad \underline{U} = (u,v) = (0,0)$ at $y=0$

(20) $\quad u(x,y = \infty) = \underline{U}_\infty(x)$,

where $\underline{U} = (u,v)$ is the velocity vector with u tangential and v normal to the boundary, ξ is the vorticity, ν the viscosity, and ∇ = gradient operator. The above equations (16)-(20) are valid for the flat plate problem, but there is no difficulty in extending them to the case of a curved wall. When this is done, it is found that these equations continue to be applicable on condition that the curvature does not change abruptly. i.e. the boundary-layer thickness is much smaller than the radius of curvature of the wall (see Chorin, Hughes, McCracken, and Marsden [11] for theoretical analysis.)

First, we derive from equations (18) and (19)

(21) $\quad v(x,y) = \dfrac{-\partial}{\partial x} \displaystyle\int_0^y u(x,y)\, dy$.

Next, from equations (17) and (20) we get

(22) $\quad u(x,y) = U_\infty(x) - \displaystyle\int_\infty^y \xi(x,y)\, dy$.

Thus, we note that once $\xi(x,y)$ is known, the velocity $\underline{U}=(u,v)$ is also known.

We now present the numerical method. Let us define our computational elements, the vortex sheets, to be surfaces of discontinuity across which the tangential velocity changes abruptly. A vortex sheet has strength ξ_i when the velocity u above and below the sheet differ by ξ_i. Each sheet is broken up into elements which participate in the approximation of the flow.

Consider a collection of vortex sheets S_i of intensity ξ_i, i=1,...,N, centered at $z_i=(x_i,y_i)$ and such that S_i is parallel to the x-axis. Using a center-difference approximation, we can approximate the tangential velocity component, using equation (22), as

$$(23) \qquad u_i = U_\infty(x_i) - \frac{1}{2}\xi_i - \sum_j \xi_j d_j \quad ,$$

where the smoothing factor $d_j = 1-|x_i-x_j|/h$ and the sum $\sum$ is over all S_j such that $y_j > y_i$ and $|x_i-x_j|<h$; h=length of the sheet. Similarly, from equation (21), for the normal velocity component v_i, we get

$$I_1 \cong U_\infty(x_i + \frac{h}{2})y_i - \sum_{j^+} \xi_j d_j^+ y_j^*$$

$$I_2 \cong U_\infty(x_i - \frac{h}{2})y_i - \sum_{j^-} \xi_j d_j^- y_j^*$$

where

$$d_j^+ = 1 - \frac{|x_i + \frac{h}{2} - x_j|}{h}$$

$$d_j^- = 1 - \frac{\left| x_i - \frac{h}{2} - x_j \right|}{h}$$

$$y_j^* = \min(y_i, y_j)$$

$\sum_+$ is over all S_j such that $0 \leq d_j^+ \leq 1$

$\sum_-$ is over all S_j such that $0 \leq d_j^- \leq 1$.

Hence

(24) $V_i = -\dfrac{(I_1 - I_2)}{h}$.

The procedure for approximating the boundary layer equations is as follows: First, we consider the corresponding inviscid boundary layer equations,

$$\xi_t + (\underline{U} \cdot \underline{\nabla}) \xi = 0$$

$$\xi = -u_y$$

$$u_x + v_y = 0 \quad .$$

The motion of the vortex sheets are approximated by

$$x_i^{n+1} = x_i^n + \Delta t \, u_i$$

$$y_i^{n+1} = y_i^n + \Delta t \, v_i$$

where Δt = time step, (x_i^n, y_i^n) is the ith-point at time $t = n \, \Delta t$, and (u_i, v_i) is the corresponding velocity vector which is computed using equations (23) and (24) above.

Next, we include the effects of viscosity by adding to the y-component of our solution an independent random variable n_i drawn from a gaussian distribution of mean zero and variance $2\nu\Delta t$. Thus,

(25) $x_i^{n+1} = x_i^n + \Delta t\ u_i$

(26) $y_i^{n+1} = y_i^n + \Delta t\ v_i + n_i$.

We see that the boundary conditions $u(x,y=\infty) = \underline{U}_\infty$ and $v(x,y=0)=0$ are automatically satisfied. The remaining boundary condition $u(x,y=0)=0$ will be satisfied through the following vorticity creation algorithm.

Suppose the velocity component tangent to the wall is $u(x,0) \neq 0$. Then the total vorticity per unit length on the wall is

$$\int_{wall}^{interior} \xi\, dy = \int \frac{\partial u}{\partial y}\, dy = u_0$$

Here y is in the direction of the normal. By antisymmetry, we continue the flow from $y > 0$ to $y < 0$, i.e., $u(x,-y)=-u(x,y)$. Choose the boundary points Q_i, $i=1,\ldots,m$ such that $\overline{Q_1 Q_2},\ldots,\overline{Q_{m-1}Q_m}$ are of length h. Since $\xi(x,-y) = \xi(x,y)$, we create at point Q_i vortex sheets S_i, $i=1,\ldots,2\ell$ such that $\sum_{i=1}^{2\ell} S_i = 2u_0$, with $|S_i|\leq\xi_{max}$ where ξ_{max} is some reasonably small quantity.

As these sheets are created, they are assigned integer tags. The effect of this tagging is to piece together the vortex elements created

at different boundary points into a single vortex sheet. Hence, the elements of the same sheet will have a unique common tag among them. Elements with the same tag are assigned the same η. Next, we let these sheets move according to the laws (25) and (26). On the average, half of the newly created sheets on the wall will flow into the upper half plane. However, to reduce the variance of the results, we require that exactly one-half of the sheets flow upwards. For this, a rejection technique is used. This technique ensures that the successive values of η have opposite signs, and upon application of formulae (25) and (26), exactly one half will flow into the lower half plane. It is for this reason that the number of vortex sheets created at any one point is an even number $= 2\ell$. For the vortex sheets in the boundary layer, but not on the wall, the antisymmetry of the flow is imposed by reflecting the sheets back into the fluid if they cross the wall. In using this algorithm, we see that the tangential boundary condition is satisfied exactly. For a detailed discussion of this method, see Chorin [10]. The computer program implementing this method together with complete documentation is presented in [5].

5. Calculation Scheme

We shall consider the calculation scheme for the following two problems.

Problem I: Consider a circular cylinder of radius 1, centered at the origin and immersed in a fluid of density 1. Partition the boundary of the circle into M equal segments each of length $h=2\pi/M$. At time $t=0$, the cylinder is started impulsively from rest with a velocity magnitude of 1. The direction of flow is parallel to the positive x-axis, therefore, in our present frame of reference the velocity at infinity is $(-1,0)$.

Problem II: Let $\tilde{z} = f(z)$ be the conformal transformation that maps the unit circle into a Joukowski airfoil of varying thickness and angles of attack. Partition the boundary of the airfoil into M segments of length h_i, $i=1,\ldots,M$. As in the case of the cylinder, the airfoil is immersed in a fluid of density 1. At time $t=0$, the airfoil is started impulsively from rest with a velocity magnitude of 1. The velocity at infinity is $(-1,0)$.

a) Flow Past a Circular Cylinder. (Problem I)

To illustrate the method, let us first consider Problem I. Immediately after time $t=0$ the tangential and normal boundary conditions are violated. To satisfy the tangential boundary condition, we first calculate the total amount of vorticity γ at the edge of the boundary layer. Then, we create a vortex sheet of strength $-\gamma$ on the boundary. By doing this, we will satisfy the tangential boundary condition and achieve a smooth transition from zero on the boundary to

the correct amount on the edge of the boundary layer. To satisfy the normal boundary condition, we use the method of images.

To be more specific, let us consider the situation at time $t = n \, \Delta t$. Let us assume that at this time, we have a collection of vortex points (x_j, y_j, k_j) centered at (x_j, y_j) of strength k_j, $j = 1, \ldots, NN$, and a collection of vortex sheets (x_i, y_i, ξ_i) with midpoints (x_i, y_i) and intensity ξ_i, $i = 1, \ldots, N$ in the flow. To satisfy the normal boundary conditions induced by the flow field, we use the method of images described in Section 3. Furthermore, we will calculate the amount of vorticity on the edge of the boundary layer when this condition is satisfied. Here the boundary layer thickness is $O(R^{-1/2})$ where R is the Reynolds number. After doing these calculations we arrive at the following result.

The complex potential for the circular cylinder problem, at time $t = n \, \Delta t$, satisfying $\underline{u} \cdot \underline{n} = 0$ is

$$w(z_i) = -\underline{U}_\infty \left(z_i - \frac{a^2}{z_i} \right) + \frac{1}{2\pi} \sum_{j=1}^{NN} i k_j \left[\log(z_i - \bar{z}_j) - \log \left(z_i - \frac{a^2}{\bar{z}_j} \right) + \log z_i \right]$$

where a is the radius of the circle and $\underline{U}_\infty = (-1, 0)$. Evaluating this expression, we get

$$u_i = 1 - \frac{(x_i^2 + y_i^2)}{(r_i^2)^2} + \frac{1}{2\pi} \sum_{j} 1 \ k_j \frac{(y_i - y_j)}{(r_{ij})^2} + \frac{1}{2\pi} \sum_{j} 2 \ k_j \frac{(y_i - y_j)}{\sigma(r_{ij})} \quad +$$

$$-\frac{1}{2\pi}\sum_{j}1\, k_j\, \frac{\left(y_i - \frac{y_j}{r_j^2}\right)}{(r_{ij}^*)^2} - \frac{1}{2\pi}\sum_{j}2\, k_j\, \frac{\left(y_i - \frac{y_j}{r_j^2}\right)}{\sigma(r_{ij}^*)}$$

$$+\frac{1}{2\pi}\sum_{j}1\, k_j\, \frac{y_i}{(r_i)^2} + \frac{1}{2\pi}\sum_{j}2\, k_j\, \frac{y_i}{\sigma(r_i)}\;,$$

$$v_i = -\frac{2x_i y_i}{(r_i^2)^2} - \frac{1}{2\pi}\sum_{j}1\, k_j\, \frac{(x_i - x_j)}{(r_{ij})^2} - \frac{1}{2\pi}\sum_{j}2\, k_j\, \frac{(x_i - x_j)}{\sigma(r_{ij})}$$

$$+\frac{1}{2\pi}\sum_{j}1\, k_j\, \frac{\left(x_i - \frac{x_j}{r_j^2}\right)}{(r_{ij}^*)^2} + \frac{1}{2\pi}\sum_{j}2\, k_j\, \frac{\left(x_i - \frac{x_j}{r_j^2}\right)}{\sigma(r_{ij}^*)}$$

$$-\frac{1}{2\pi}\sum_{j}1\, k_j\, \frac{x_i}{(r_i)^2} - \frac{1}{2\pi}\sum_{j}2\, k_j\, \frac{x_i}{\sigma(r_i)}\;,$$

where

$$r_i = \sqrt{x_i^2 + y_i^2}$$

$$(r_i)^2 = (x_i^2 + y_i^2)$$

$$r_{ij} = \sqrt{(x_i - y_j)^2 + (y_i - y_j)^2}$$

$$r_{ij}^* = \sqrt{\left(x_i - \frac{x_j}{r_j^2}\right)^2 + \left(y_i - \frac{y_j}{r_j^2}\right)^2}$$

$$(r_j)^2 = x_j^2 + y_j^2$$

σ = cut-off to be determined later

$\sum_1$ is taken over all vortices such that $r_i, r_{ij}, r_{ij}^* > \sigma$

$\sum_2$ is taken over all vortices such that $r_i, r_{ij}, r_{ij}^* \leq \sigma$.

Note that at time $t = 0$, the above formulae yield

$$u_i = 1 - \frac{(x_i^2 + y_i^2)}{(x_i^2 + y_i^2)^2} \quad \text{which is} = 0 \text{ on the boundary } \partial D,$$

$$v_i = \frac{-2x_i y_i}{(x_i^2 + y_i^2)^2} \neq 0 .$$

We want v_i to be zero on the boundary ∂D. The velocity vector is $\underline{U}_i = (u_i, v_i) = (0, v_i)$ on the boundary. The resulting vorticity is $\underline{U}_i \cdot \underline{\tau} = 2\xi \neq 0$. This is twice the amount because of the contribution due to the image points. This factor of 2 is exactly the factor needed when we use the vortex sheet method as described in Section 4. Initially, at time $t=0$, the amount to be created at each point on the boundary is exactly $-2\xi_0$ unless $|-2\xi_0| < \xi_{min}$, where ξ_{min} is some very small quantity. In this case, for computational economy, no sheets are created. Upon appropriate modification of the rejection technique for equations (25) and (26), exactly one-half of what has just been created will disappear into the object. Thus, the boundary condition is satisfied exactly except for the times when $|2\xi_0| < \xi_{min}$.

At time $t=n\Delta t$ we create an amount ξ_{diff} which is the difference between the amount required and the amount already existing in the boundary layer. In this way, 1) the transition from ξ on the edge of the boundary layer to zero on the boundary is achieved and 2) the tangential boundary condition is satisfied.

After all the new sheets are created, they all move according to the laws (25) and (26). As stated before, exactly one-half of the newly created sheets will walk into the object and will be lost. The

rest of the sheets become points if they flow outside of the boundary layer. Since sheets and points are determined by the same parameters, this change is simple and straightforward, i.e., (x_i, y_i, ξ_i) becomes (x_i, y_i, k_i) where $k_i = h\xi_i$. Thus, when a vortex sheet becomes a vortex point, the only change is in the intensity of the point to satisfy conservation of circulation. To preserve antisymmetry, the sheets in the boundary layer (but not on the boundary) that flow into the object are reflected to their image points. We know a priori that the sheets with sharp gradients are close to the point of separation. As a programming tool, we can test the velocity ratio u/v of the sheets and change them into points if u/v is greater than some chosen parameter determined by the geometry of the obstacle in the flow.

Transitions from vortex points to vortex sheets follow a similar procedure. A point can become a sheet if it either flows back into the boundary layer or if it flows into the object and its image point lies in the boundary layer. In the latter case, the point is reflected as a sheet. One can argue that if Δt were more refined, this point will end up in the boundary layer as it follows its trajectory. Thus, when it flows into the object as a sheet, it will automatically be reflected to preserve antisymmetry. Note that this cannot be done if the image point is not in the boundary layer, for we only have this antisymmetry property for the boundary layer equations. This procedure, suggested by Chorin, yields a non-trivial improvement in the accuracy of the model. A similar hybrid algorithm was presented by Chorin for two and three dimensional calculations applied to the analysis of the boundary layer over a flat plate in 1980 [12].

The only remaining task now is to determine the value of the cut-off σ . We approach this problem in the following way. Consider a collection of vortex blobs. If these blobs are close to the boundary of the object, the effects of their interaction with the boundary should be the same as the effects of the interaction of the vortex sheets with the boundary. In other words, the cut-off should have the value that will not only give fast convergence, but also smooth transition from vortex sheets to vortex blobs.

Thus, let us consider the following example in determining the cut-off. Let the line $y=0$ be a wall, and consider the flow to be in the upper half plane. The boundary layer thickness is $O(R^{-1/2})$. Let there be a vortex sheet of intensity ξ situated at point z_1 at the edge of the boundary layer. Also, let a vortex blob with the same circulation (i.e., of intensity ξh) be situated at the same point z_1. The image vortex is thus at $\bar{z}_1$. Let z_2 be the point on the boundary such that the segment $\overline{z_1 z_2}$ is normal to the boundary. If we choose $\sigma = h/\pi$, we can verify from formula (11) that the velocity at z_2 induced by the blob at z_1 and its image at $\bar{z}_1$ is

$$u_2 = 2 \left(\frac{1}{2\pi} \xi h \; \frac{y - y_1}{\sigma r} \right) \quad ,$$
$$= \left(\frac{1}{\pi} \xi h \; \frac{1}{(h/\pi)} \right)$$
$$= \xi , \qquad\qquad v_2 = 0 \quad .$$

This shows that the boundary cannot distinguish between a vortex blob and a vortex sheet. Thus, as vortex blobs approach the edge of the

boundary layer, their effects on the boundary coincide with the effects of the sheets on the boundary. We can, therefore, view the computational elements as sheets near the boundary and as blobs far away from the boundary. Hence, $\sigma = h/\pi$ is the value for the cut-off which is consistent with our numerical method.

b) <u>Flow Past Airfoils</u> (Problem II)

In computing the flow field around an airfoil, we can either do our calculations in the physical plane (the plane that contains the airfoil) or in the mapped plane (the plane that contains the circle, after the airfoil is mapped into the circle). Calculations in the physical plane follow closely the process described in the above discussion since the method is essentially independent of the geometry of the obstacle. The major differences are 1) the bookkeeping is a much bigger project since we cannot rely on the nice properties of the circle and 2) we must replace the method of images by a potential solver (see Section 3). In making calculations in the mapped plane, we can take advantage of the geometry of the circle. However we must adjust our calculations to coincide with the solution obtained from calculations in the physical plane.

6. On the Self-Interaction of Vortices Under Conformal Maps

From the analysis on the cut-off σ, we see that if we choose $\sigma = \pi/h$ in the physical plane, the effects of points and sheets coincide at the edge of the boundary layer. However, when "smoothing" is carried out in the mapped plane, a correction term must be subtracted off in the original plane. Let us determine this correction term. Consider a point vortex with strength k_0 situated at $z = z_0 \epsilon \Gamma$, where Γ is a region of the z-plane with boundary $\partial\Gamma$. (See Figure 2.)

FIGURE 2

strength k_0

z_0

Γ

$\partial\Gamma$
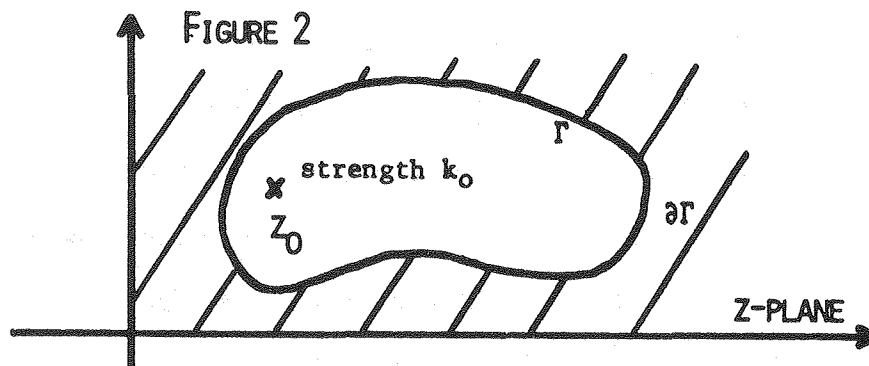
Z-PLANE

Let $(u(z), v(z))$ be the velocity field in Γ having 1) zero normal compo-
nent along $\partial\Gamma$ and 2) correct circulation ($=k_0$) along curves in Γ
which have z_0 in their interior.

Let $(u_0(z), v_0(z))$ be the velocity field induced in the z-plane by
the point vortex at z_0.

We want to find the "self-induced velocity of the point vortex in
presence of boundaries," defined as

$$\lim_{z \to z_0} \quad (u(z), v(z)) - (u_0(z), v_0(z)) \quad .$$

Let $W(z)$ be a conformal mapping of Γ onto the upper half plane $(\text{Im } W \geqslant 0)$.
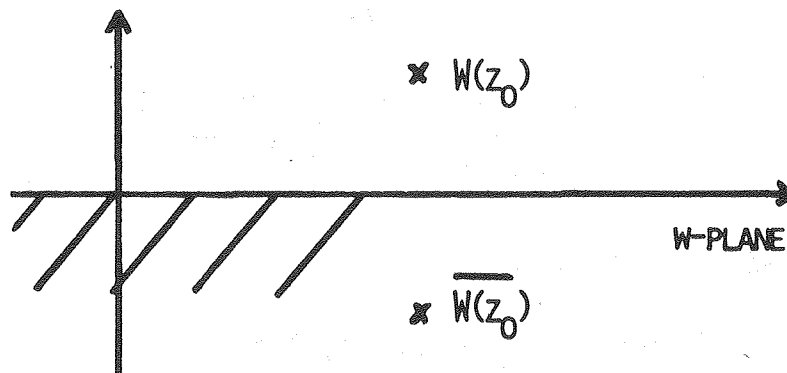
Then, $(u(z), v(z))$ is, by potential theory,

$$u(z) - iv(z) = W'(z)\, (\mu(z) - i\gamma(z))$$

where $\mu - i\gamma$ is the velocity at $W(z)$ in the w-plane (see equation (15)). The velocity at $W(z)$ due to a point vortex at $W(z_0)$ and a point vortex at $\overline{W(z_0)}$, both of strength k_0, is

$$\mu(z) - i\gamma(z) = \frac{k_0}{2\pi i} \left\{ \frac{1}{W(z) - W(z_0)} - \frac{1}{W(z) - \overline{W(z_0)}} \right\} .$$

The velocity $(u_0(z), v_0(z))$ due to vortex at point z_0 is simply

$$u_0(z) - iv_0(z) = \frac{k_0}{2\pi i} \left(\frac{1}{z - z_0} \right) .$$

Now,

$$[(u(z)-iv(z))-(u_0(z)-iv_0(z))]$$

$$= \frac{k_0}{2\pi i}\left\{\frac{W'(z)}{(W(z)-W(z_0))} - \frac{W'(z)}{W(z)-\bar{W}(z_0)} - \frac{1}{z-z_0}\right\}$$

$$= \frac{k_0}{2\pi i}\left\{\frac{W'(z)(z-z_0)-(W(z)-W(z_0))}{[W(z)-W(z_0)]\,(z-z_0)} - \frac{W'(z)}{W(z)-\bar{W}(z_0)}\right\}.$$

The Taylor Expansion of $W(z)-W(z_0)$ is

$$W(z)-W(z_0) = W'(z)(z-z_0) - \frac{1}{2}W''(z)(z-z_0)^2 + \cdots .$$

Substituting into above we get

$$= \frac{k_0}{2\pi i}\left\{\frac{W'(z)(z-z_0)-W'(z)(z-z_0)+\frac{1}{2}W''(z)(z-z_0)^2+\cdots}{[W(z)-W(z_0)]\,(z-z_0)} - \frac{W'(z)}{W(z)-\bar{W}(z_0)}\right\}$$

$$= \frac{k_0}{2\pi i}\left\{\frac{\frac{1}{2}W''(z)+0(z-z_0)}{\left(\dfrac{W(z)-W(z_0)}{z-z_0}\right)} - \frac{W'(z)}{W(z)-\bar{W}(z_0)}\right\}$$

Hence

$$\lim_{z\to z_0}[(u(z)-iv(z)) - (u_0(z)-iv_0(z))]$$

$$= \lim_{z\to z_0}\frac{k_0}{2\pi i}\left\{\frac{\frac{1}{2}W''(z)+0(z-z_0)}{\left(\dfrac{W(z)-W(z_0)}{z-z_0}\right)} - \frac{W'(z)}{W(z)-\bar{W}(z_0)}\right\}$$

$$= \frac{k_0}{2\pi i}\left\{\frac{\frac{1}{2}W''(z_0)}{W'(z_0)} - \frac{W'(z)}{W(z_0)-\bar{W}(z_0)}\right\}$$

"Smoothing in the mapped plane" would only give the second term above. Hence, in order to obtain the correct value for u(z) and v(z), we need to add on the correction term

$$\frac{-k_0}{2\pi i} \left(\frac{\frac{1}{2} W''(z_0)}{W'(z_0)} \right) .$$

This term can be neglected only when $W''(z_0) = 0$. The above analysis is due to Ilkka Karasalo [23].

7. Derivation of the Lift and Drag Formula Due to Pressure

The formula we used in our numerical program to calculate the lift and drag is

$$L_p - iD_p = \rho \frac{\partial}{\partial t} \sum_{j=1}^{N} \Gamma_j \left(w_j - \frac{1}{w_j^*} \right)$$

L_p is the value of the lift, D_p is the value of the drag, Γ_j is the strength of the vortex point situated at $w_j = (x_j, y_j)$, and w_j^* is the image vortex. The derivation of the formula is as follows. Blasius Formula:

$$(27) \qquad \frac{p}{\rho} + \frac{1}{2} q^2 + \phi_t = \text{constant} \qquad\qquad \text{[Bernoulli]}$$

where $q = |u - iv| = |d\Phi/dz|$.

Now

$$L_p - iD_p = \oint p \, dz \doteq -\frac{\rho}{2} \left\{ \oint q^2 dz + 2 \frac{\partial}{\partial t} \oint \phi dz \right\}$$

The integral $\oint q^2 dz$ can be evaluated by noting that

$$\oint q^2 dz = \left\{ \oint \frac{d\Phi}{dz} \left(\frac{d\Phi}{dz} \right)^* dz^* \right\}^*$$

$$= \left\{ \oint \frac{d\Phi}{dz} \, d\Phi^* \right\}^*$$

But in view of the tangency condition, $d\Phi$ is real at the surface so that $d\Phi^* = d\Phi$. Thus, we have

$$\oint q^2 dz = \left| \oint \frac{d\Phi}{dz} d\Phi \right|^* = \left| \oint \left(\frac{d\Phi}{dz}\right)^2 dz \right|^*$$

so that

$$(28) \qquad L_p - i\,D_p = -\frac{\rho}{2} \left| \oint \left(\frac{d\Phi}{dz}\right)^2 dz \right|^* - \rho \frac{\partial}{\partial t} \oint \phi\,dz \quad .$$

For steady flow this reduces to the familiar form (Blasius' Formula)

$$D_p - i\,L_p = \frac{i\rho}{2} \oint \left(\frac{d\Phi}{dz}\right)^2 dz \quad .$$

Now Equation (27) is not valid for rotational flow in general. The general form is

$$(29) \qquad \frac{\partial}{\partial t} \underline{u} \cdot d\underline{s} + \text{grad} \left(p/\rho + \frac{1}{2} q^2\right) d\underline{s} = -\sqrt{v_n}\,\omega ds$$

where the right side represents the rate at which vorticity is crossing the contour. The contour direction is anticlockwise and $\sqrt{v_n}$ is the outward normal flow. The inviscid model of the flow is as follows:

1. vorticity: $\frac{D\omega}{Dt} = 0$

2. continuity: $\nabla \cdot \underline{u} = 0$

3. boundary conditions:
    a. $\underline{u} \cdot \underline{n} \geqslant 0$ at surface
    b. $\oint_{S_\infty} \underline{u} \cdot d\underline{s} = 0$
    c. $\underline{u} \sim (U_\infty, 0)$ as $z \geqslant \infty$
    d. $\omega \underline{u} \cdot \underline{n} \geqslant \frac{d}{dt}(\underline{u} \cdot \underline{s})$ at surface $+ \epsilon$.

We wish to apply (29) near the body (say at distance ϵ from the surface), such that $\epsilon \ll \ell$ (ℓ characterizes the body), but $\epsilon \gg \delta$ (the boundary-layer thickness). We assume that the pressure at the contour differs from that at the body by $O(\epsilon)$ or, at least $O(1)$ as $\epsilon \to 0$. We

further assume that, on the contour $\underline{u} \cdot \underline{n} = O(\epsilon)$, but that $\omega \underline{u} \cdot \underline{n} = O(1)$. All of the terms in (29) contribute.

Consider the form of (29) for point vortices whose velocities are $O(1)$. Then $\underline{u} = \nabla \phi$ and we have from (29)

$$\frac{d}{ds} \left(\phi_t + \frac{p}{\rho} + \frac{1}{2} q^2 \right) = - \sqrt{v_n}(s) \, \omega(s) \quad .$$

Now $\sqrt{v_n}(s)\omega(s)$ is the vorticity source for the fluid exterior to the contour. Since ω is in the form of point vortices,

$$\int_t^{t+\Delta t} \sqrt{v_n}(s)\omega(s)dt = \sum_k \Gamma_k \, \delta(s - s_k) = \sum_k \Gamma_k \frac{d}{ds} \mathcal{H}(s-s_k)$$

where the sum is over those vortices crossing the contour between t and $t + \Delta t$. It is assumed that the contour location and time step Δt preclude multiple crossings within a time step. δ is the Dirac function, s_k is the crossing point of the vortices, and $\mathcal{H}$ is the corresponding Heaviside function. Then

$$\frac{d}{ds} \left(\phi_t + \frac{p}{\rho} + \frac{1}{2} q^2 + \frac{1}{\Delta t} \sum_k \Gamma_k \mathcal{H}(s - s_k) \right) \approx 0$$

so that [as $\Delta t \to 0$, $\Gamma_k \to 0$, such that $\frac{1}{\Delta t}\Sigma \Gamma_k = O(1)$],

$$\frac{p}{\rho} + \phi_t + \frac{1}{2} q^2 + \frac{1}{\Delta t} \sum_k \Gamma_k \mathcal{H}(s - s_k) = \text{constant} \quad .$$

Then

$$L_p - i D_p = - \frac{\rho}{2} \left\{ \oint q^2 dz + 2 \frac{\partial}{\partial t} \oint \phi dz + \frac{2}{\Delta t} \sum_k \Gamma_k \oint \mathcal{H}(s-s_k) dz \right\}$$

to within $O(\epsilon)$. Now for every vortex between the contour and the body there is an image vortex within $O(\epsilon)$ of it. The potential of the pair is

$$- \frac{i}{2\pi} \log \frac{w - w_j}{w - \frac{1}{w_j^*}} = - \frac{i}{2\pi} \log \frac{w - w_j}{w - w_j + \left(w_j - \frac{1}{w_j^*} \right)} \qquad .$$

Note: the body is a circle in the w-plane. If the body is a circle in the z-plane, then $w = z$,

$$\sim \frac{-i}{2\pi} \log \left(1 - \left(w_j - \frac{1}{w_j^*} \right) \right) = O(\epsilon) \ , \ \text{for} \ w - w_j = O(1) \quad .$$

We then ignore all vortices between the body and the contour (and their images). Now,

$$J \equiv \left\{ \oint q^2 dz \right\}^* = \oint \left(\frac{d\Phi}{dz} \right)^2 dz = \oint \left(\frac{d\Phi}{dw} \right)^2 \frac{dw}{dz} dw$$

where both $d\Phi/dw$ and dw/dz have singularities within the contour. We assume that the poles of these two functions do not coincide. Since dw/dz is analytic exterior to the unit circle we transform variables $X = w^{-1}$ so that

$$J = \oint \left(\frac{d\Phi}{dw} \right)^2 \frac{dw}{dz} \frac{dX}{X^2} \quad .$$

Now

$$\frac{d\Phi}{dw} = 1 - w^{-2} - \frac{i}{2\pi} \sum_j \Gamma_j \left(\frac{1}{w-w_j} - \frac{1}{w-\frac{1}{w_j^*}} \right)$$

$$= 1 - X^2 - \frac{i}{2\pi} \sum_j \left(\frac{Xw_j^*}{X-w_j^*} - \frac{Xw_j^{-1}}{X-w_j^{-1}} \right) \Gamma_j$$

Then $\frac{1}{X} \frac{d\Phi}{dw}$ is analytic within the unit circle except at $X=0$ and $X=w_j^{-1}$, $j=1,2,\ldots$, where it has simple poles, so that

$$\left(\frac{1}{X} \frac{d\Phi}{dw} \right)^2 = \left[\frac{1}{X} - X - \frac{i}{2\pi} \sum_j \Gamma_j \left(\frac{w_j^*}{X-w_j^*} - \frac{w_j^{-1}}{X-w_j^{-1}} \right) \right]^2$$

has double poles at $X=0$ and at $X=w_j^{-1}$ as well as simple poles at $X=w_j^{-1}$ (the simple pole at $X=0$ is removable).

$$J = \oint \left\{ \frac{1}{X^2} - 2 + X^2 - \frac{i}{\pi} \left(\frac{1}{X} - X \right) \sum_j \Gamma_j \left(\frac{w_j^*}{X-w_j^*} - \frac{w_j^{-1}}{X-w_j^{-1}} \right) \right.$$

$$\left. - \frac{1}{4\pi^2} \sum_j \sum_k \Gamma_j \Gamma_k \left(\frac{w_j^*}{X-w_j^*} - \frac{w_j^{-1}}{X-w_j^{-1}} \right) \left(\frac{w_k^*}{X-w_k^*} - \frac{w_k^{-1}}{X-w_1^{-1}} \right) \right\} \mathcal{D}(X) \, dX$$

where

$$D(w) = \mathcal{D}(X) = \mathcal{D}\left(\frac{1}{w} \right) \quad .$$

Summing Residues:

The terms independent of Γ have no residue (D. Alembert's paradox). The term linear in Γ gives

$$\underline{J_2 = 2\pi i \left\{ \frac{i}{\pi} \sum_k \Gamma_k (1 - w_k^{-2}) D(w_k) \right\}} \quad .$$

The quadratic terms give

$$J_3 \equiv \oint \frac{1}{4\pi^2} \sum_j \sum_k \Gamma_j \Gamma_k \left(\frac{w_j^* w_k^{-1}}{(X-w_j^*)(X-w_k^{-1})} + \frac{w_k^* w_j^{-1}}{(X-w_k^*)(X-w_j^{-1})} \right) \mathcal{D}(X)\, dX$$

$$= \frac{2\pi i}{4\pi^2} \left\{ \sum_j \Gamma_j w_j^* \sum_k \frac{\Gamma_k w_k^{-1}}{w_k^{-1}-w_j^*} D(w_k) + \sum_k \Gamma_k w_k^* \sum_j \frac{\Gamma_j w_j^{-1}}{w_j^{-1}-w_k^*} D(w_j) \right\}$$

$$= \frac{2\pi i}{2\pi^2} \left\{ \sum_j -\Gamma_j \sum_k \frac{\Gamma_k}{w_k - \frac{1}{w_j^*}} D(w_k) \right\} = \frac{2\pi i}{2\pi^2} \sum_k \Gamma_k\, D(w_k) \sum_j \frac{-\Gamma_j}{w_k - \frac{1}{w_j^*}}$$

$$J_4 \equiv \oint -\frac{1}{4\pi^2} \sum_j \sum_{k \neq j} \Gamma_j \Gamma_k \frac{w_j^{-1} w_k^{-1}}{(X-w_j^{-1})(X-w_k^{-1})} \mathcal{D}(X)\, dX$$

$$= -\frac{2\pi i}{4\pi^2} \left\{ \sum_j \Gamma_j w_j^{-1} \sum_{k \neq j} \frac{\Gamma_k w_k^{-1} D(w_k)}{w_k^{-1} w_j^{-1}} + \sum_k \Gamma_k w_k^{-1} \sum_{j \neq k} \frac{\Gamma_j w_j^{-1} D(w_j)}{w_j^{-1}-w_k^{-1}} \right\}$$

$$= -\frac{2\pi i}{2\pi^2} \left\{ \sum_j \Gamma_j \sum_{k \neq j} \frac{\Gamma_k D(w_k)}{w_j - w_k} \right\} = \frac{2\pi i}{2\pi^2} \sum_k \Gamma_k\, D(w_k) \sum_{j \neq k} \frac{-\Gamma_j}{w_k - w_j}$$

Then

$$\frac{J}{2} = -\sum_k \Gamma_k\, D(w_k) \left\{ 1 - w_k^{-2} - \frac{i}{2\pi} \sum_{j \neq k} \Gamma_j \left(\frac{1}{w_k-w_j} - \frac{1}{w_k - \frac{1}{w_j^*}} \right) + \frac{i}{2\pi} \frac{\Gamma_k}{w_k - \frac{1}{w_k^*}} \right\}$$

$$= -\sum_k \Gamma_k V_k$$

where V_k is the complex velocity in the z-plane at the center of vortex k, so that

$$\oint q^2\, dz = -2 \sum_k \Gamma_k\, V_k^*$$

Now

$$\oint \phi \, dz = \oint \Phi z - \oint z \, d\Phi = \oint \Phi z - \oint z \frac{d\Phi}{dw} \, dw \qquad .$$

Again, we map to the X plane since the $z \to w$ mapping is analytic exterior to the unit circle. Then,

$$\oint z \frac{d\Phi}{dw} \, dw = \oint z \frac{d\Phi}{dw} \frac{dX}{X^2}$$

$$= \oint \left\{ 1 - X^2 - \frac{i}{2\pi} \sum_j \Gamma_j \left(\frac{Xw_j^*}{X - w_j^*} - \frac{Xw_j^{-1}}{X - w_j^{-1}} \right) \right\} \frac{Z(X) \, dX}{X^2} \qquad .$$

Now since $Z \sim W$ as $W \to \infty$, $Z(X) \sim 1/X$ as $X \to 0$.

Summing residues:

$$\oint z \frac{d\Phi}{dw} \, dw = -2\pi i + \sum_j \Gamma_j \left(w_j - \frac{1}{w_j^*} \right) - \sum_j \Gamma_j z_j \qquad ,$$

so that

$$\oint \phi \, dz = 2\pi i + \sum_j \Gamma_j \left(z_j - z_0 - w_j + \frac{1}{w_j^*} \right)$$

where z_0 is the end point of the integration, so that

$$\frac{\partial}{\partial t} \oint \phi \, dz = \frac{\partial}{\partial t} \sum_j \Gamma_j \left(z_j - z_0 - w_j + \frac{1}{w_j^*} \right) \qquad .$$

Now we need to evaluate the integral

$$\oint \Omega \, dz \quad \text{where} \quad \frac{d\Omega}{ds} = \sqrt{v_n}(s)\omega(s) \qquad .$$

Now

$$L_p - i D_p = \rho \sum_j \Gamma_j V_j^* - \rho \frac{\partial}{\partial t} \sum_j \Gamma_j \left(z_j - z_0 - w_j + \frac{1}{w_j^*}\right) - \rho \oint \Omega \, dz \quad ,$$

where

$$\oint \Omega \, dz = \oint \Omega z - \oint z \, d\Omega = \oint \Omega z - \oint z \frac{d\Omega}{ds} \, ds$$

$$= \oint \Omega z - \oint z \sqrt{v_n} \omega \, ds \quad ,$$

now

$$\oint \Omega = \oint \sqrt{v_n} \omega \, ds = \frac{\partial}{\partial t} \sum_j \Gamma_j$$

so that

$$\oint \Omega z = \frac{\partial}{\partial t} \sum_j \Gamma_j z_0$$

and since

$$\frac{\partial}{\partial t} \sum_j \Gamma_j z_j \sim \sum_j \Gamma_j V_j^* + \oint z \sqrt{v_n} \omega \, ds$$

we get (for the limit below)

$$(30) \quad L_p - i D_p \sim \rho \frac{\partial}{\partial t} \sum_j^N \Gamma_j \left(w_j - \frac{1}{w_j^*}\right)$$

$$\text{as} \quad \left. \begin{array}{c} \Gamma_j \to 0 \\ N \to \infty \end{array} \right\} \quad N\Gamma_j = O(1) \quad .$$

The above formula and analysis are due to Rogallo [43]. Another derivation of $L_p - i D_p$, similar to the above, can be found in [18].

8. Numerical Experiments for Flow Past a Circular Cylinder

    a) Numerical Parameters

In all of the numerical calculations done on the circular cylinder problem, the boundary of the circle is divided into M=20 pieces, each of length $h=2\pi/M$. The circle has radius r=1. The Reynold's number is R=1000, mainly because there are many experimental studies with which to compare the results. Also, at this value one can be sure to observe the separating streamlines of the flow clearly.

The cylinder is impulsively set into motion at time t=0, where t is measured in nondimensional units. Δt is chosen to be 0.2. Numerical experiments were done with $\Delta t=0.2$ and $\Delta t=0.1$ and with all the other parameters kept fixed. Refining Δt does not improve the calculations significantly, i.e., when we compare the calculated lift and drag coefficients with these choices of Δt, the average value of the lift and drag is changed by less than one percent.

For reasons of economy, we choose ξ_{max} as large as possible, but not so large that we loose the main features of the problem. After some experimentation $\xi_{max}=1.0$ was chosen. Note that a sheet of length h and strength ξ_{max} will eventually become a blob of strength $= h \cdot \xi_{max}$. For the values of h and ξ_{max} chosen as above, this means that the value 0.31415 is the maximum strength for each blob.

A flow started impulsively from rest goes through a long transitional period before it becomes fully developed. We found that at time t=8, the flow is leaving the transitional period and entering into the

stage of fully developed flow. At this time, we refine our calcula-
tions by taking ξ_{max} to be 0.2. The main reason for this is to
produce a more accurate model which will predict the point of separa-
tion very accurately. Changing ξ_{max} to an even smaller quantity, say
$\xi_{max}=0.1$, after time t=8 did not improve the results significantly.
Again, the results corresponding to $\xi_{max}=0.1$ and $\xi_{max}=0.2$ after
time t=8 differ from each other by less than a percentage point.

   b) <u>Development of the Flow</u>

   Figures 3 through 5 show different stages of the development of the
flow with $\xi_{max}=1.0$ until time t=8 than $\xi_{max}=0.2$; h=2π/M, M=20,
σ=π/h, R=1000, and Δt=0.2. This development compares well with
physical experiments (see [3] and [41]).

   Initially after impulsive start, diffusion outweighs convection.
However, after a short time, the convection of vorticity becomes more
significant than the diffusion of vorticity, especially in the direc-
tion of the flow parallel to the cylinder. The vorticity created to
satisfy the boundary condition is carried by this convection to the
rear of the cylinder. This vorticity created is negative in sign on
the upper surface and positive on the lower surface. Ultimately there
is more vorticity of each sign at the rear of the cylinder than is
needed to satisfy the no-slip condition there and a backflow is induced
near the surface. The backflow counters the forward-moving fluid and
deflects it away from the rear of the cylinder. Most of the fluid
passing close to the cylinder appears to gather itself into two
discrete lumps, or eddies, at the rear of the cylinder. (See Figure 3

corresponding to time t=2). At time t=2, we see that the eddies in the wake of the cylinder are just beginning to take form. By time t=5, we see that the eddies are well developed and the points of separation are about 85° from the forward stagnation point on both sides. The streamlines leave the body tangentially at the points of separation. (See Figure 4). Furthermore, new eddies are being formed while the original ones have convected downstream. The region enclosed by the two separating streamlines grows larger and is even larger than the cylinder itself. By time t=8, the eddies created earlier are merging due to diffusion. (See Figure 5.) At time t=11, the flow is asymmetric and the points of separation can be estimated from the graph to be around 78° and 115° from the forward stagnation point.

Ultimately, one of the eddies at the rear of the cylinder will break loose from the cylinder and move downstream. This departure of so much vorticity from the neighborhood of the cylinder will affect the flow near the cylinder. The remaining eddy of the opposite rotation will consequently become larger, and eventually this eddy will also shed. The shedding of the eddies causes asymmetry in the flow pattern, asymmetry in the two points of separation, and causes dips and rises in the lift and drag coefficients. The numerical experiments we ran were stopped on or before time t=11. This is not enough time for the flow to develop a vortex street with more than one oscillation. Hence, Strouhal numbers were not calculated in this study.

c) Lift and Drag Coefficients

The lift and drag coefficients are calculated using the formula (30)

$$L - iD = \rho \frac{\partial}{\partial t} \sum_{j=1}^{N} \Gamma_j \left(z - \frac{1}{z*}\right)$$

with

$$D = C_D(\rho U^2/2)A, \quad L = C_L(\rho U^2/2)A \quad .$$

Here L is the value of the lift, D is the drag, Γ_j is the strength of the vortex point situated at $z_j=(x_j,y_j)$, z_j^* is the image vortex, A is the characteristic length, and ρ = density = 1. The values of L and D are averaged over time. At time t=8, the average drag coefficient is C_D=1.055 which is less than 2 percent from the experimental value of 1.04. The lift coefficient C_L = -0.098 is very close to zero, the desired average value. Assuming that the flow is developed at t=8, the following momentum defect equation is also used in calculating the drag coefficient at this time:

$$(31) \qquad D_2 = F_X = - \rho U_\infty \int U dy$$

where the integration is taken from y=-5 to y=+5, and U_∞=freestream velocity. See Landau and Lifshitz [26].

Using the first formula, we have, after averaging over time t=11, C_D=1.01 and C_L = -0.14. Formula (31) above gives us C_{D2} = 1.01, where C_{D2} is averaged over 15 time steps from t=8 to t=11. The behavior of the drag can be seen in Figure 6. It starts at 1.01, climbs sharply to about 1.4 corresponding to impulsive start, and then oscillates about the point 1.0 with a variance of 0.036. The lift starts at zero, rises to 0.1, and then becomes slightly negative for most of

the time until t=5.6. It then oscillates with varying amplitudes
staying almost always between ±1, with an average which is slightly
below zero at time t=11, and with a variance of 0.100. The last dip
in the lift coefficient corresponds to the changing flow pattern around
the cylinder, and to the shedding of an eddy at the rear of the
cylinder. (See Figure 7.) For more on experimental values of drag,
see Sighard [49].

A run of this duration takes on the average between 3.5 and 4
minutes on the CDC-7600 at Lawrence Berkeley Laboratory. This flow at
time eight is modeled by a total of 467 elements. After this time a
greater number of points are generated at each time step corresponding
to the refinement ξ_{max}=0.2. At time eleven, there are 908 points
and 176 sheets. For a comparative study using different numerical
methods to model flow past circular cylinders, see Nahavandi and
Chen [38], and Sarpkaya and Schoaff [44]. Also, for experimental and
numerical results related to this problem, see [15], [16], [51], [6],
and [7].

45
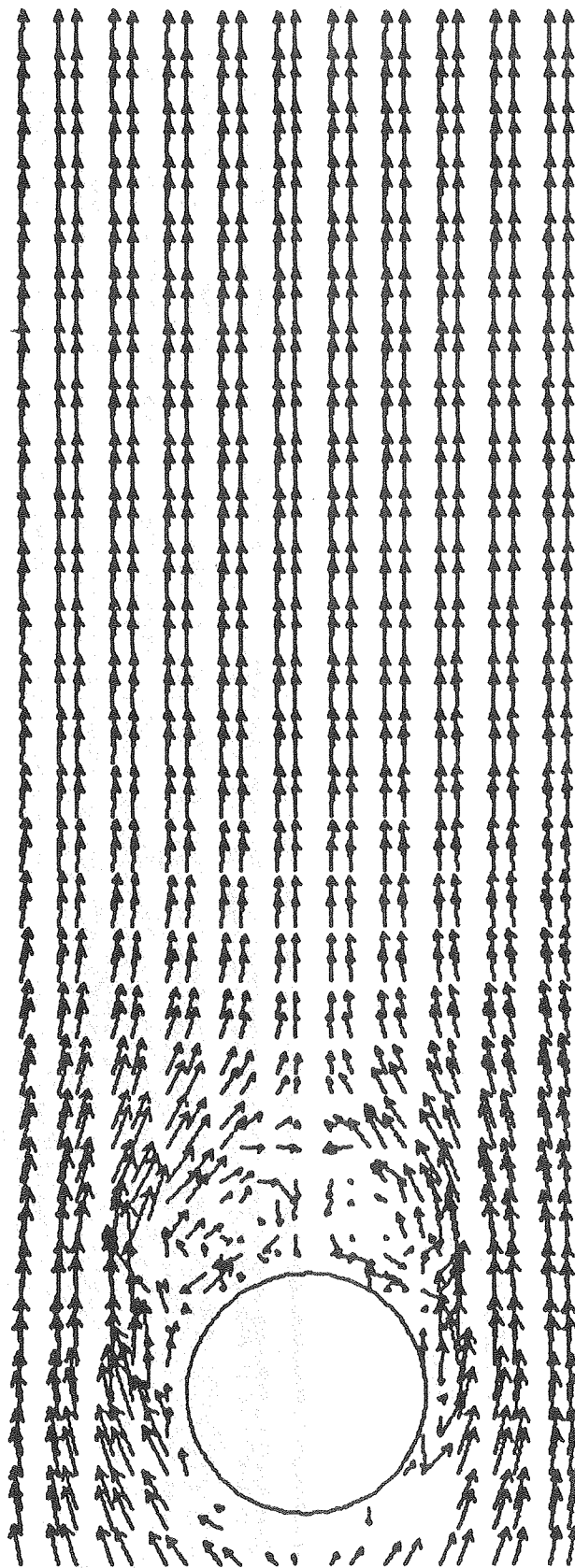
FIGURE 3

TIME T = 2

FIGURE 4

TIME T = 5

Figure 5

Time τ = 8

TIME T = 11

48
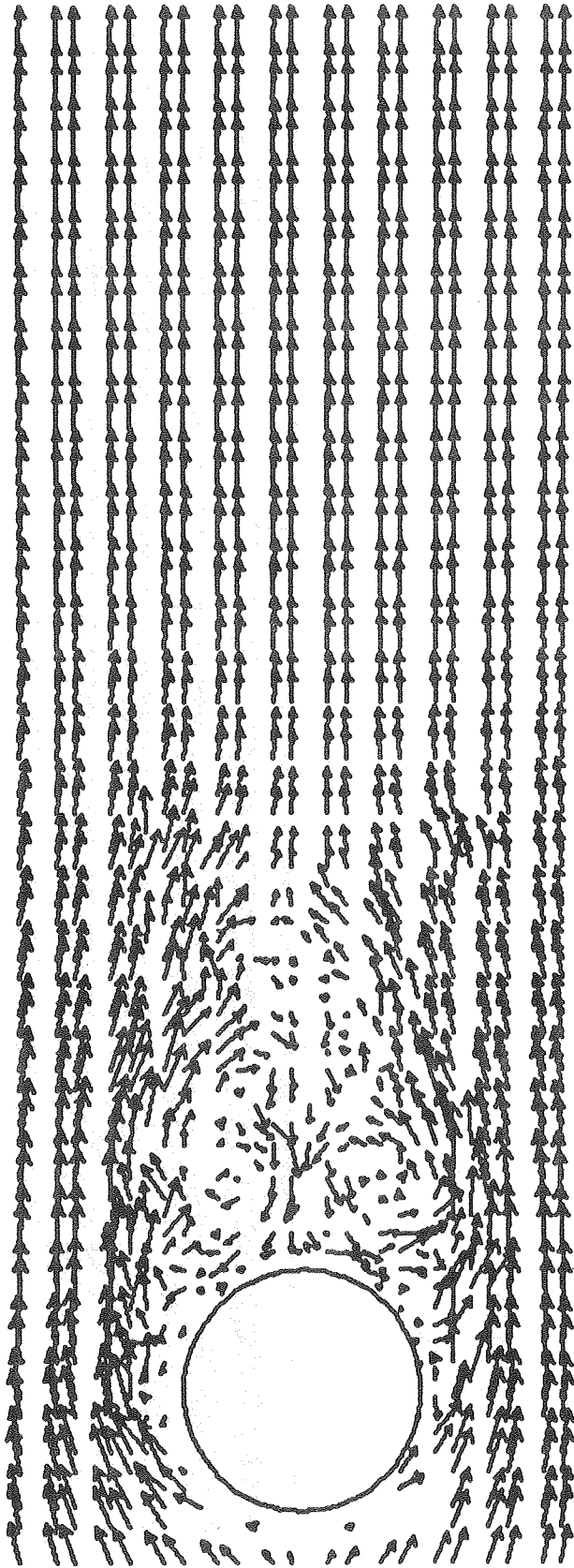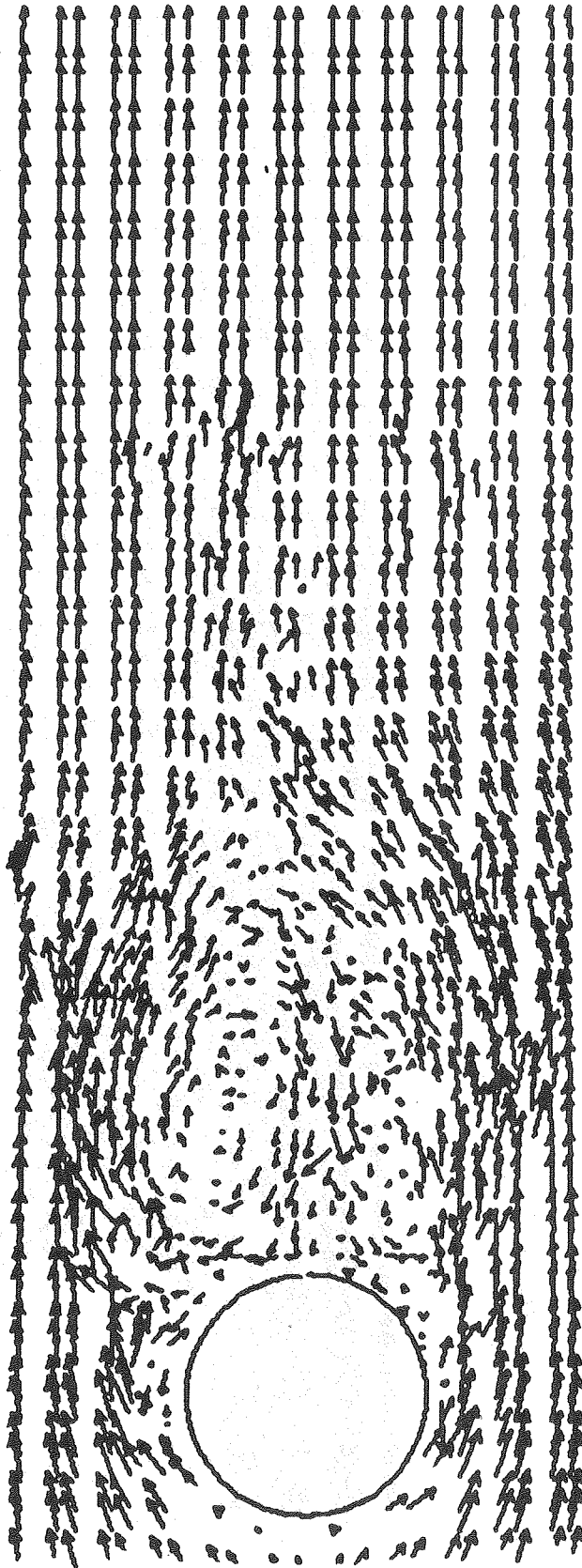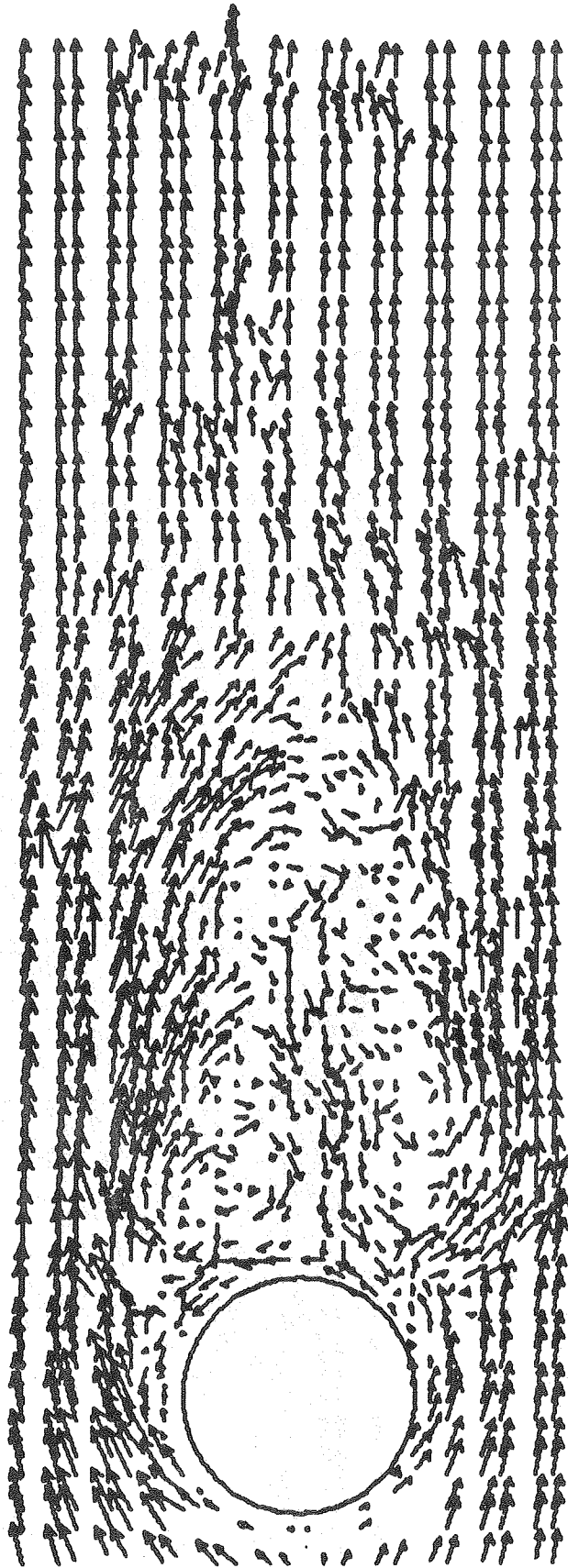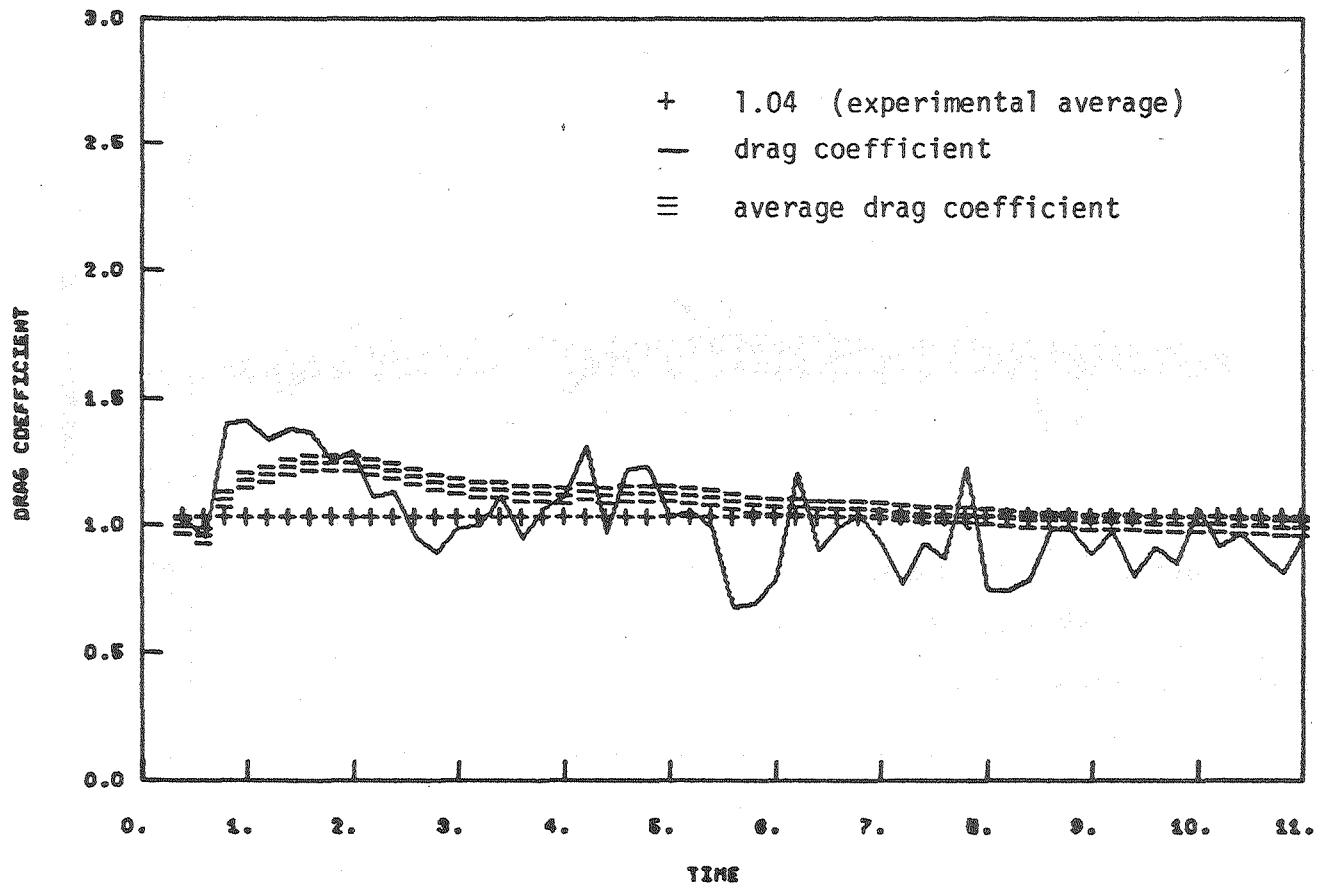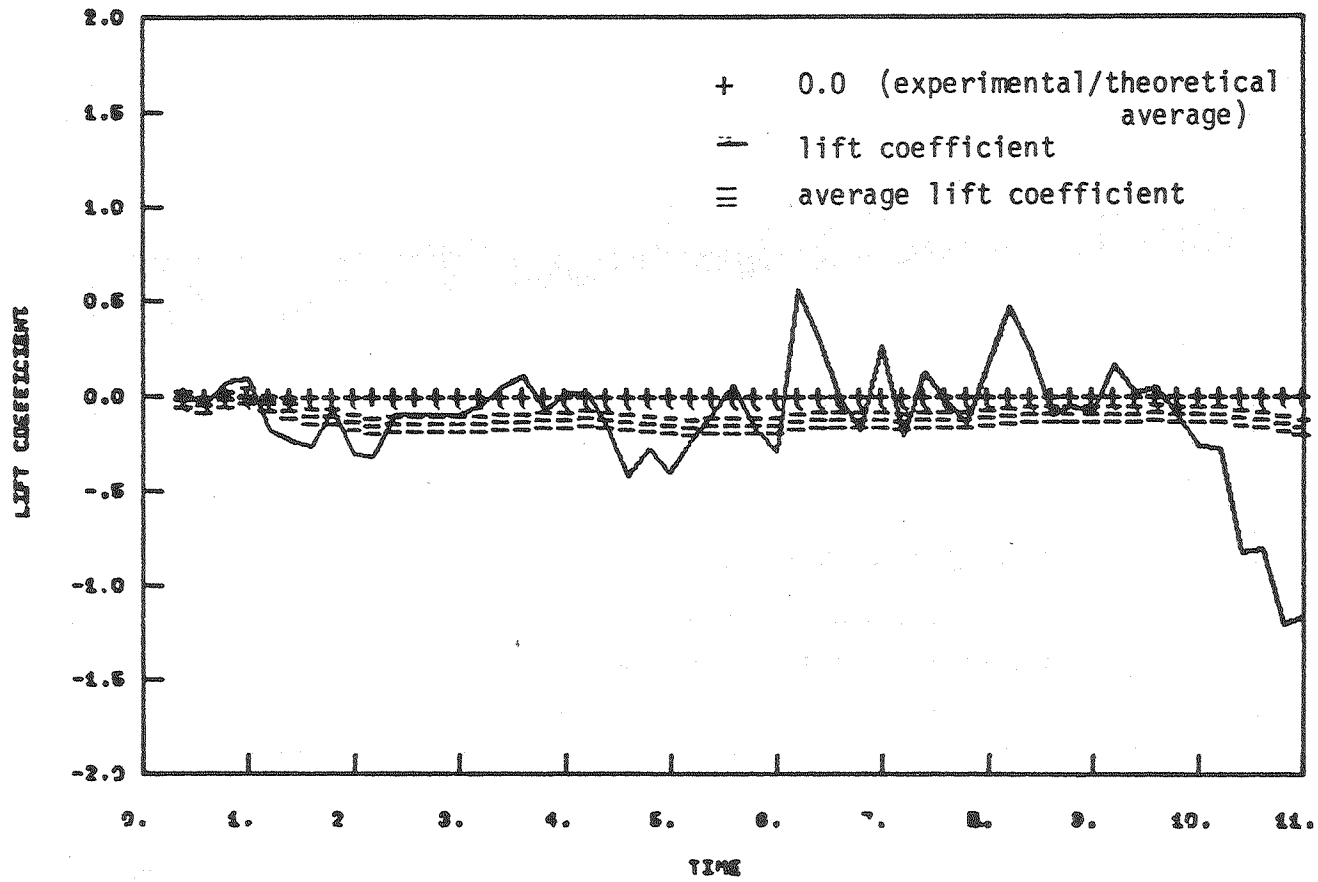
FIGURE 6

FIGURE 7

9. Flow at the Trailing Edge of an Airfoil

a) Treatment of the Map at the Trailing Edge

Consider the following conformal map which transforms a circle of radius (1+a) into a symmetric Joukowski airfoil:

$$(32) \quad \tilde{z} = f(z) = \frac{1}{(1+a)} \left(z + \frac{1}{z} \right) e^{-i\alpha}$$

where $z = -a + (1+a)e^{i\theta}$, $0 \leq \theta \leq 2\pi$, $a \in R$. (see Figure 8). The parameter a controls the shape of the airfoil, and the parameter α controls the angle of attack.

FIGURE 8
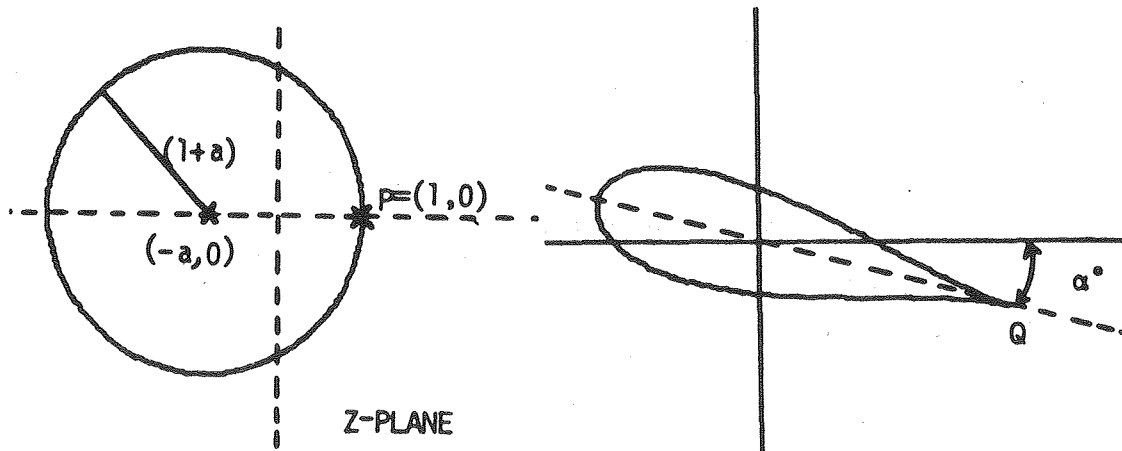
Z-PLANE

Let P be the point which is mapped into the trailing edge Q of the airfoil. If $(u_q - i v_q)$ is the velocity at Q in the profile plane, we have

$$u_q - i v_q = (u_p - i v_p)/f'(z)$$

where

$$f'(z) = \frac{1}{(1+a)} \left(1 - \frac{1}{z^2}\right) e^{-i\alpha} \qquad .$$

At the point $z=(1,0)$ we see that $f'(z) = 0$. Thus, $(u_q - iv_q)$ is infinite at the trailing edge. Therefore, we have a singularity at the sharp end of the airfoil. The other singularity is at point $z=(-1,0)$. This point transforms into a point inside the airfoil, and therefore produces no problems to our flow.

However, in the physical problem, the flow at the trailing edge is a stagnation point (see Figure 9). Thus, at point $z=(1,0)$ it follows that $(u_p - iv_p)=(0,0)$. Using this information, we see that at $z=(1,0)$ we have

$$(u_q - iv_q) = (u_p - iv_p)/f'(z) = 0/0.$$

Applying l'Hospital's rule we see that the singularity at the trailing edge is removable since

$$\frac{d}{dz}\left\{ (u_p - iv_p)/f'(z) \right\} \qquad \text{is finite at } z=(1,0) \quad .$$

To make the trailing edge a stagnation point corresponding to the physical flow, we add to the potential flow a circulation term. This term depends on the orientation of the airfoil, and is chosen so that the stagnation point and the velocity peak at the sharp edge 'cancel' each other. For this value of the circulation, the velocity is finite at the trailing edge. For more information on the theory of wings see references [1], [2], and [42] and for information on how to determine the circulation term, see [37].

FIGURE 9
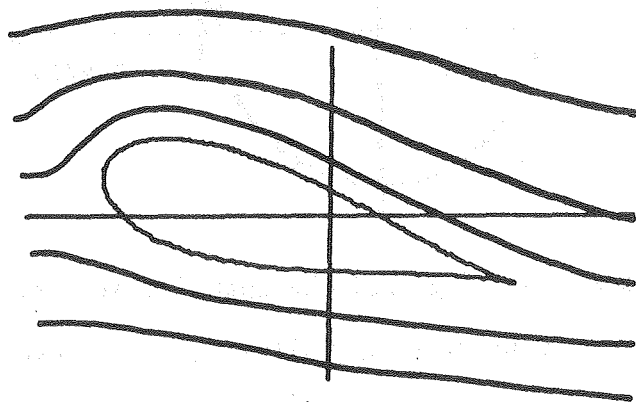
b) Treatment of the Sheets at the Trailing Edge

Consider the problem of flow past a circular cylinder of radius 1 centered at the origin. Assume that there is a sheet of length h situated at point $z_i=(1,\epsilon)$ tangential to the obstacle (see Figure 10). In the circular plane, the effect of a sheet is calculated by subtracting the shadow of the sheet projected normally onto the boundary. Thus, a sheet with its center at point z_i close to the x-axis will effect the fluid both above and below the axis. Recall that a vortex sheet is a sheet of discontinuity, where the velocity above and below the sheet differs by ξ_i, where ξ_i is the strength associated with the sheet located at z_i. Each sheet tends to slow the fluid velocity in the tangential direction.

FIGURE 10
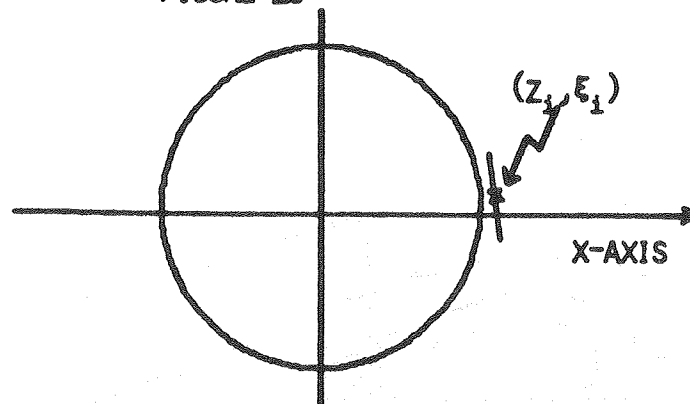
Under our conformal mapping (32) the sheet located at z_i in the circle plane will be mapped into the following configuration in the airfoil plane.

FIGURE 11
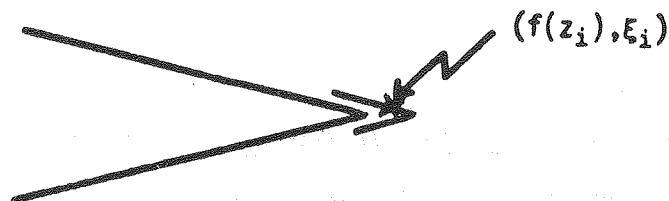
When we calculate the contribution to the boundary condition from this sheet, we see that this sheet affects both sides of the airfoil. It simultaneously slows the fluid velocity on top and on the bottom of the airfoil. Thus, the effect of this sheet is felt across the solid boundary. This is not physically possible.

Instead, we do the following. Consider the sheet located at point $z_i=(1,\epsilon)$ in the circle plane. The center of this sheet is above the x-axis, therefore, the transformed point $f(z_i)$ lies on the top of the

airfoil. The sheet whose center is $f(z_i)$ lies in the direction of the streamlines. The streamlines of the flow do not bend over the trailing edge. Thus, vortex sheets lying in the direction of the streamlines should not be allowed to bend over the trailing edge. Hence, the correct configuration in the airfoil plane corresponding to the sheet situated at $z_i=(1,\varepsilon)$ in the circle plane, is as shown in Figure 12.

FIGURE 12

$(f(z_i),\xi_i)$
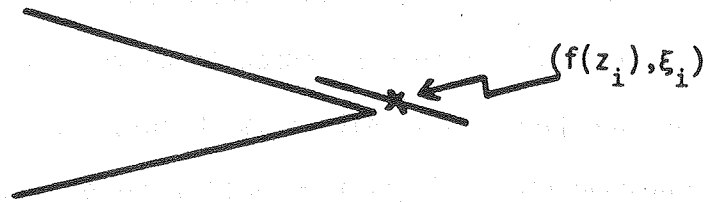
To calculate the contribution of this sheet to the boundary condition we project this sheet onto the boundary in the direction normal to the boundary. We can easily see that this sheet casts no shadow onto the lower part of the boundary. The contribution of this sheet to the boundary condition is thus restricted to the top part of the airfoil. The portion of the sheet that does not cast a shadow onto the boundary of the object acts in exactly the same way as the portion of the sheet that does cast a shadow onto the boundary of the object. The only difference is that the portion of the sheet that casts no shadow has no effect on the boundary condition of the airfoil. When this sheet flows out of the boundary layer, it becomes a vortex point of strength $\xi_i h_i$.

10. Numerical Experiments for Flow Past Airfoils

a) Numerical Parameters

In calculating flow past an airfoil, the following conformal mapping was used:

$$\tilde{z} = f(z) = \frac{1}{(1+a)} \left(z + \frac{1}{z} \right) e^{i\alpha} \quad .$$

Again, the parameter a determines the shape of the airfoil and the parameter α controls the angle of attack. Note that the solution to the irrotational flow is not uniquely determined. In this study, the solution to the potential flow was chosen to be the one that gives zero velocity at the trailing edge. With this choice, the fluid leaves the cusped trailing edge tangentially from both sides of the airfoil. This is done by adding the appropriate circulation term to the fundamental solution to the potential equation. For a given orientation of the airfoil, this circulation should have the value such that the rear stagnation point is located at the sharp trailing edge. By choosing the circulation to have the value that will make the trailing edge a stagnation point, we minimize the amount of work required to achieve steady flow. For information on how to determine the value of the circulation, see Milne-Thomson [37].

Numerical calculations for the potential component of the velocity were carried out in the circle plane, and Routh's theorem was applied to obtain the corresponding velocity in the airfoil plane. The creation of vorticity and the random walk components of the algorithm were calculated in the airfoil plane.

The numerical parameters for the airfoil problem were chosen to be the same as for the case of the problem of flow past a circular cylinder. The parameters that varied in the problem of flow past an airfoil are a and α. The parameter a changes the thickness of the airfoil and the parameter α changes the angle of attack. In each case, the boundary of the circle was divided into M=20 pieces, each of length h=2π/M. Under the conformal mapping, the airfoil was therefore also divided into M=20 pieces each of length $h_i = h \cdot |f'(z_i)|$. When a vortex sheet flowed out of the boundary layer, it became a vortex blob of strength equal to $h_i \cdot \xi_i$. Once again, ξ_{max}=1.0, R=1000 and Δt=0.2.

b) Development of the Flow

Case I: i) a = 0.50 α = 0.00   R = 1000

          ii) a = 0.25 α = 0.00   R = 1000

i) An airfoil is started impulsively from rest in an infinite pool of fluid of density 1. The flow at infinity relative to the moving air-foil is (-1,0). Initially, we have a potential flow where the stream-lines close to the body closely follow the boundary, and separate at the rear stagnation point. Immediately afterwards, a vortex sheet is formed around the airfoil. This vorticity diffuses and is washed downstream by convection. As in the case of the circular cylinder, there will eventually be more vorticity at the rear end than is needed to satisfy the boundary conditions there, and backflow develops. This happens sometime before time t=2 (see Figure 13). By time t=3, a vortex bubble is seen to be forming at the bottom of the rear stagnation

point. The points of separation have moved forward toward the front half of the airfoil, and are separating asymmetrically about the airfoil. This corresponds to the oscillatory pattern at the wake of the airfoil. At this time, we note that the velocity magnitude of the vortices are stronger on the top of the airfoil than on the bottom side of the airfoil (see Figure 14). At time t=5, the circular vortex bubble, visible at the bottom side of the rear stagnation point, has become quite strong. The velocity magnitude of the vorticies are now stronger at the bottom side of the airfoil than at the top. This faster velocity will eventually carry the eddy downstream, away from the airfoil. When this happens, the velocity on the top will become stronger and the points of separation will shift positions. At this time, the points of separation are asymmetric, separating in the front half of the airfoil. The streamlines leave the body tangentially from these points. The velocity magnitude of the vortices in the wake of the airfoil is on the average close to 1, which is the freestream velocity. This observation holds true for all the numerical experiments (see Figure 15).

ii) We now change the parameter a to 0.25 while keeping all other values fixed. For this problem, we see that a similar flow development occurs (see Figures 16 and 18). The points of separation begin to move forward shortly after impulsive start and separate asymmetrically about the airfoil. An oscillatory pattern at the wake of the airfoil develops and is seen to have started before time t=2.

FIGURE 13   TIME τ = 1

TIME τ = 2

Figure 14   Time t = 3

60
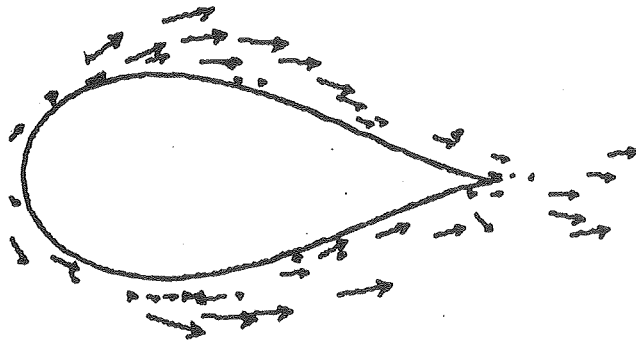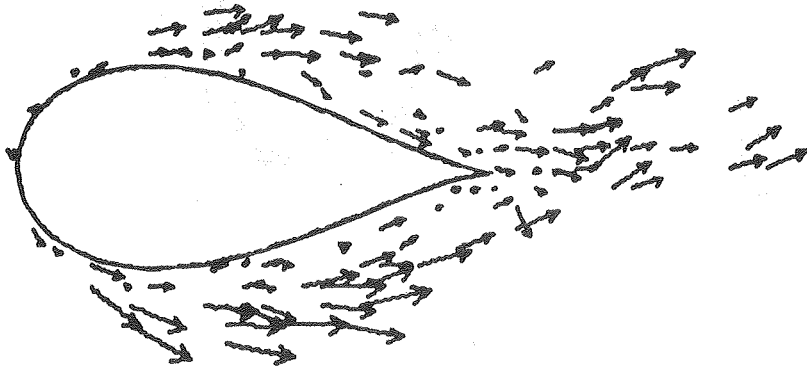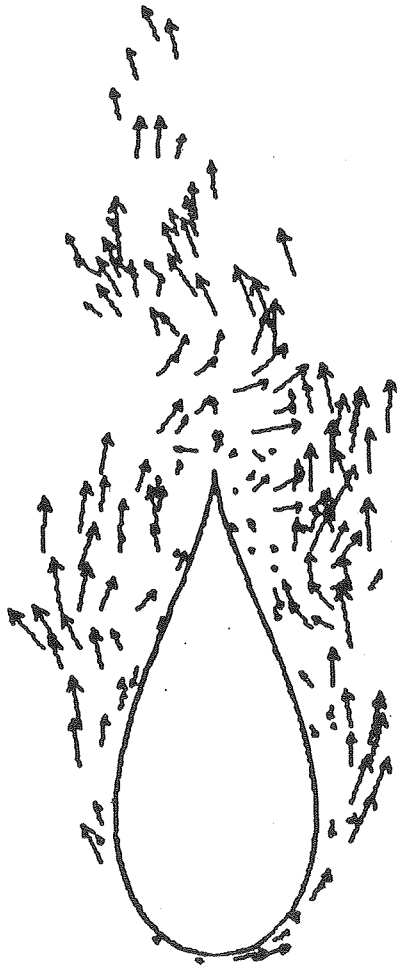
FIGURE 15   TIME τ = 5
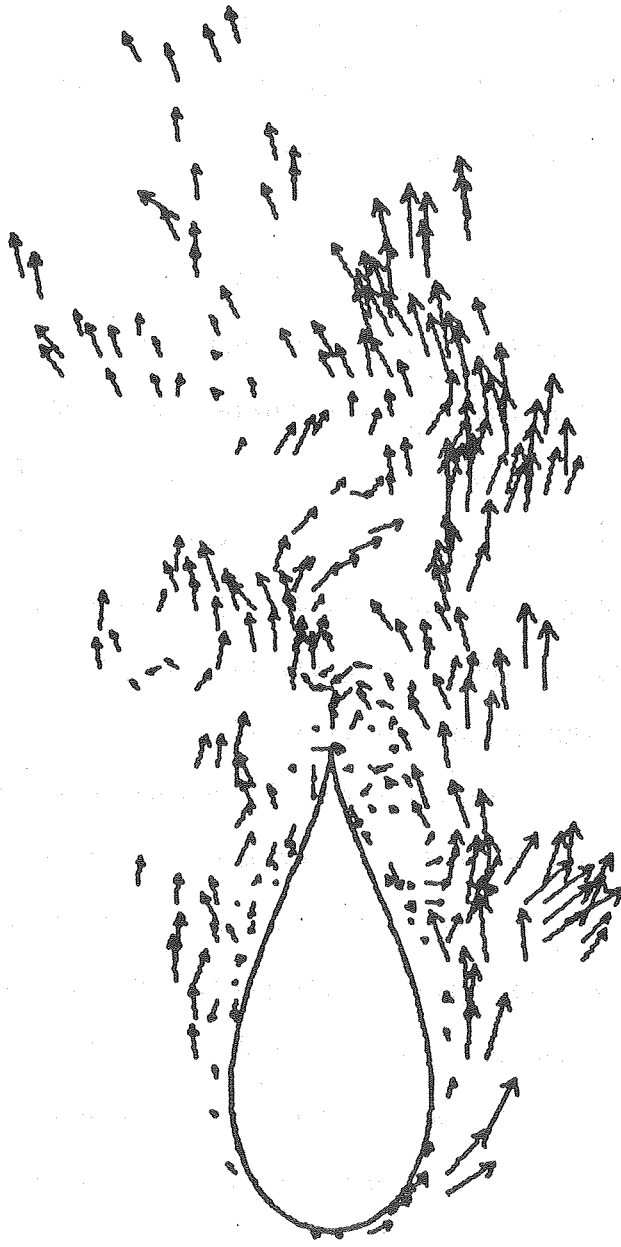
For this run we computed the drag and lift coefficients using formula (30). Figure 19 shows the development of the drag coefficient. It starts at zero at time t=0, climbs up rapidly because of the impulsive start of the airfoil, and oscillates between 0 and 1.5, leaving an average of 0.78. The lift coefficient starts at zero, stays essentially zero until time t=0.6, then oscillates about zero staying always between ±1. The lift coefficient averages to -0.09 after time t=5. This is only slightly different from the theoretical value of $C_L=0.0$ (see Figure 20).

This run and each of the subsequent runs took on the average 68 CP-seconds on the CDC-7600 at Lawrence Berkeley Laboratory. At time t=5, the flow was modeled by approximately 70 sheets and 300 points.

Case II: i) a = 0.25 $\alpha = -\pi/12$ R = 1000

            ii) a = 0.25 $\alpha = -\pi/12$ R = 5000

i) In this numerical calculation, an airfoil tilted at an angle of $-\pi/12$ radians is started impulsively from rest. The Reynolds number is 1000, and the fluid density is 1.

The flow is initially potential and without circulation, where the point of separation on the top of the airfoil does not coincide with the trailing edge. Immediately after the impulsive start, the top point of separation moves to the rear. The velocity as an average is greater above the body than below it. Therefore, different amounts of vorticity are created and shed from the top and from the bottom. As a result circulation is produced around any contour surrounding the body.

FIGURE 16   TIME τ = 2

FIGURE 17   TIME τ = 4

FIGURE 18   TIME T = 5

64

FIGURE 19

drag coefficient ———

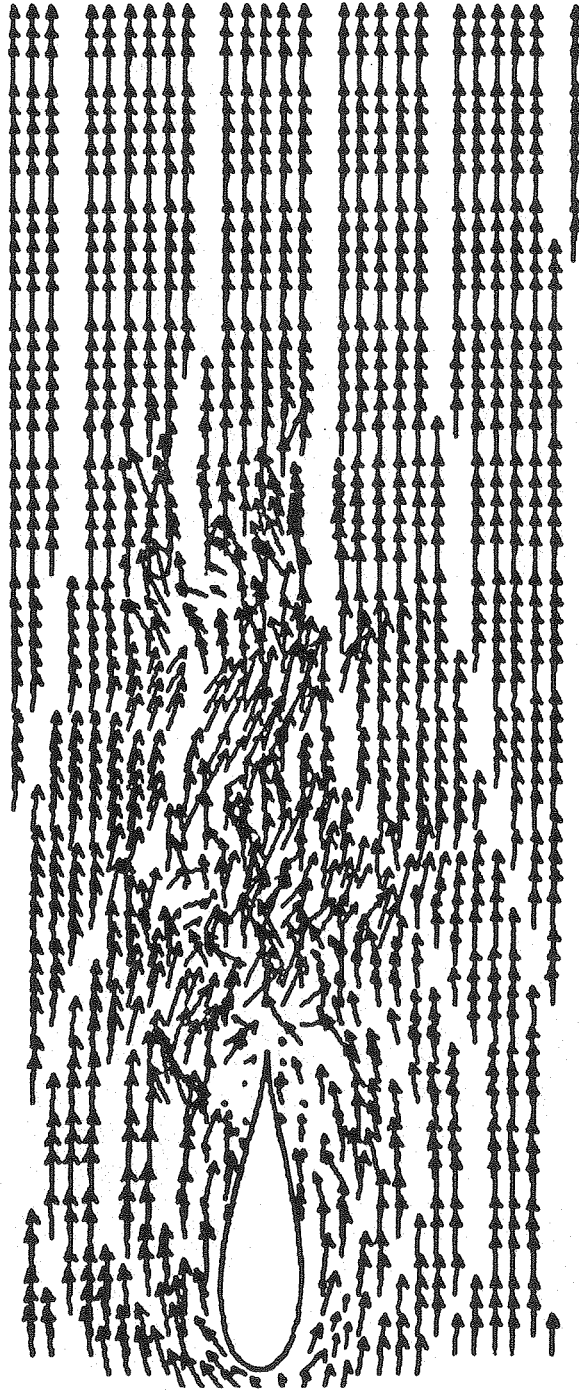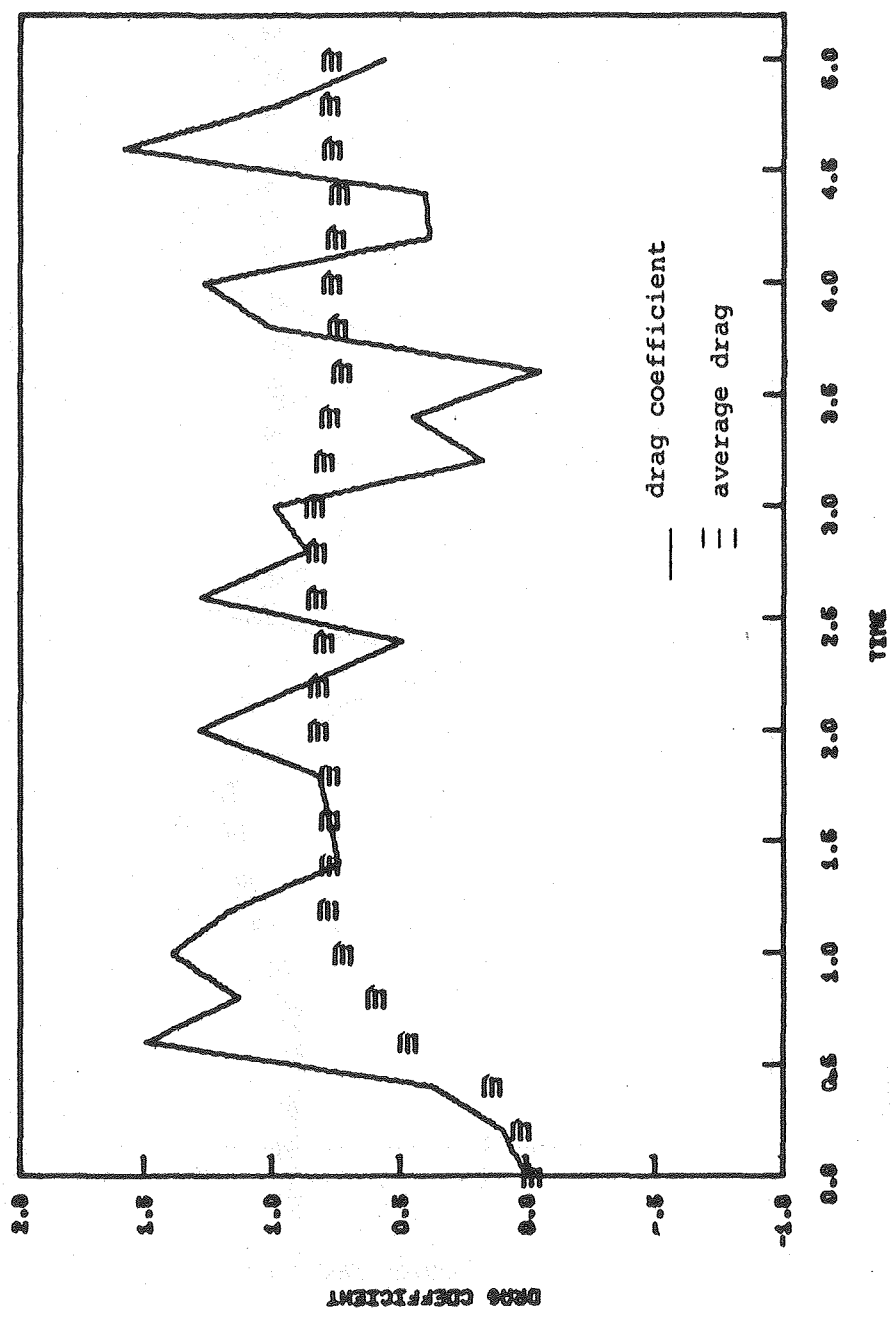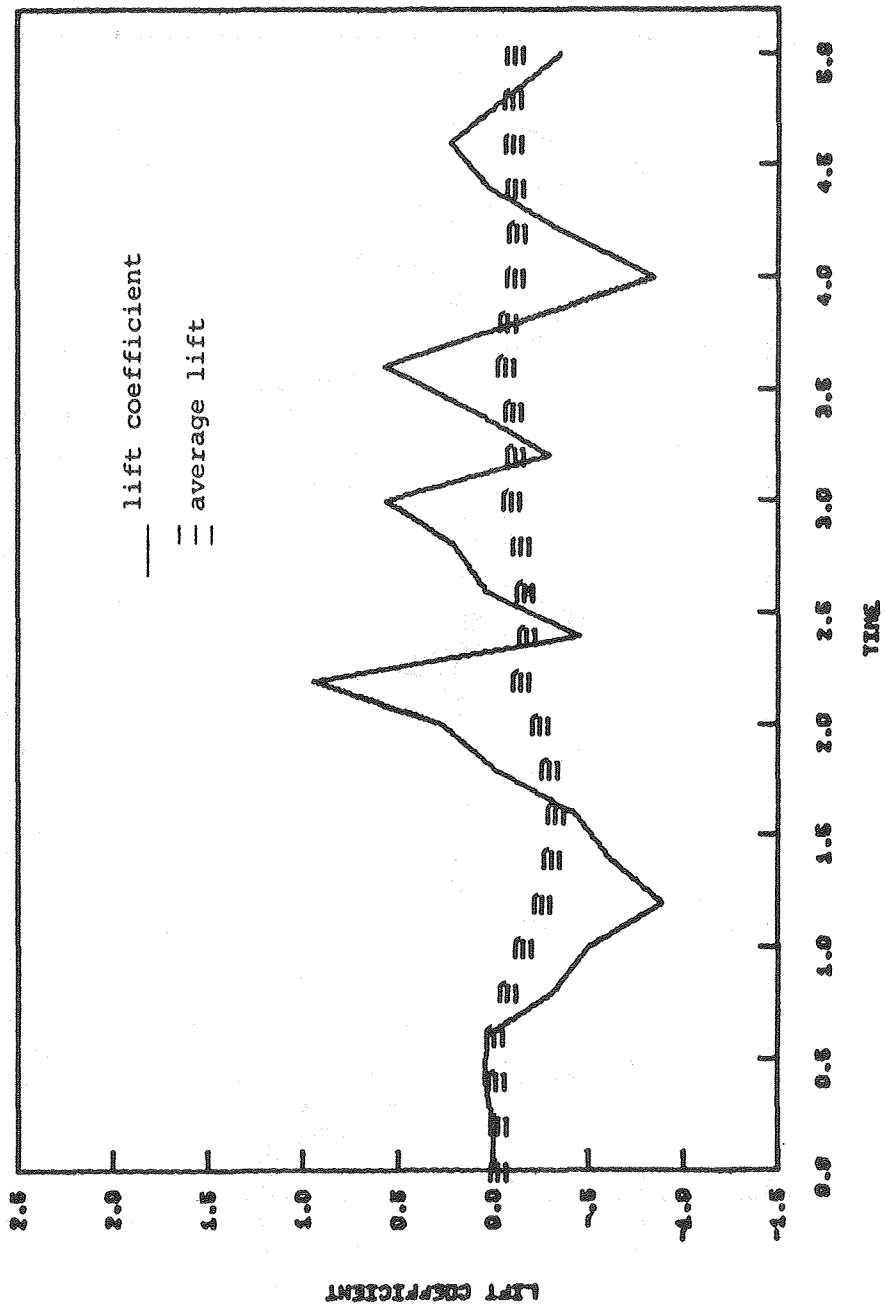average drag ═══

TIME

DRAG COEFFICIENT
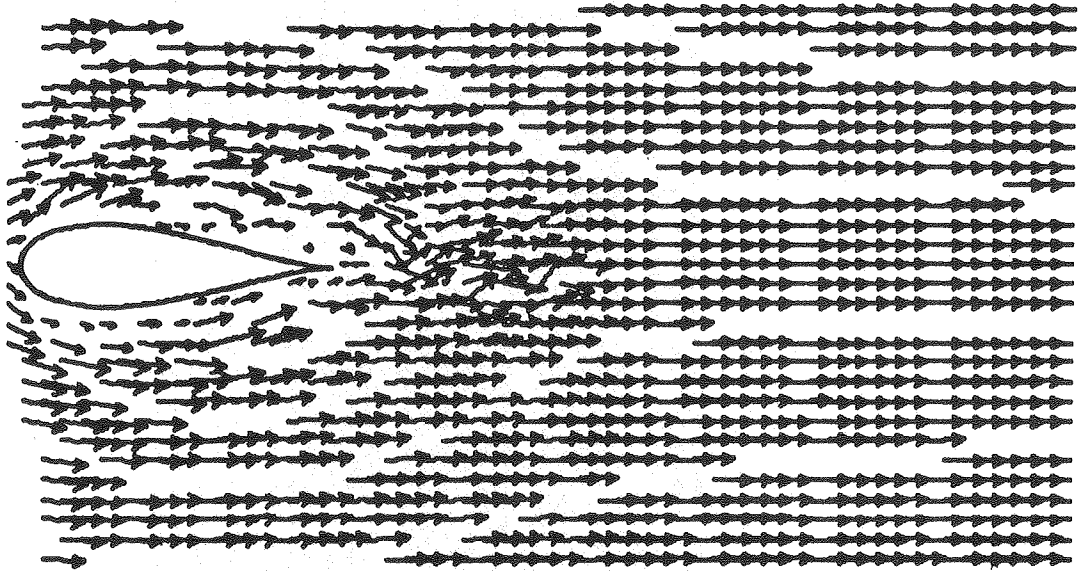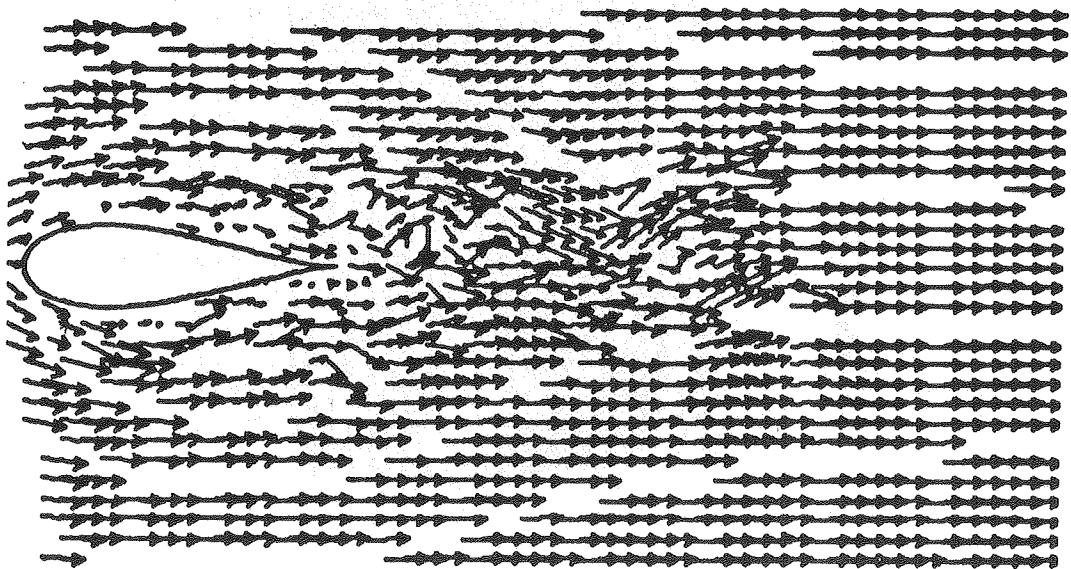
FIGURE 20

FIGURE 20

When the motion is started from rest, thin vortex layers of unequal strength leave the top and the bottom, thus causing circulation to grow. The vortex layers unite at the tail end of the airfoil.

Backflow develops almost immediately after the point of separation coincides with the trailing edge. Consequently the point of separation is pushed back up towards the front of the airfoil. At time $t=1$, the top separation point is half way up the airfoil (see Figure 21). The bottom point of separation is very close to the rear and remains there. The streamlines leave the points of separation tangentially. The flow at the trailing edge behaves very smoothly and leaves the body tangentially there.

The vorticity created at the boundary first diffuses, then is carried downstream by convection and finally is shed from the edge by the fluid. So, continual generation of vorticity at the boundary is necessary to satisfy the no-slip condition. The deceleration of the fluid close to the body, and the acceleration of the fluid above, cause the fluid to collect into circular patterns in the area downstream from the top separation point (see Figures 22 to 25). These circular patterns get larger and stronger as they roll down the airfoil. Eventually the vorticity in these circular eddies is shed off the tail end of the airfoil into the wake. There is not a continuous shedding of these eddies. The concentration of the vorticity in the wake is therefore not uniform.

At time $t=5.4$ we see that the flow on the top of the airfoil separates very close to the leading edge of the airfoil. The vorticity

in the flow downstream from this point causes the formation of circular eddies. The eddies are larger farther downstream. The flow in the bottom part of the airfoil separates at the trailing edge. The vorticity in the wake is not uniform and generates an oscillatory pattern (see Figure 25).

The flow due to an impulsive start of an airfoil at an angle of attack equal to $-\pi/12$ radians, in a fluid of Reynolds number 1000, has been previously studied by Metha and Lavan [34] and by Wu, Sampath and Sankar [56]. The former solved the problem numerically using a finite difference method while the latter used an integro-differential formulation. There are several differences between their calculations and those in this study. Besides the obvious differences in numerical methods used, the conformal map used is also different, and their calculations were carried out to a longer distance past the airfoil. Their figures of the flow development were traced using streamlines. Thus, it is difficult to compare the creation, diffusion and convection of the vorticity. However, interpolation from the graphs exhibited in their papers, we see that the flow pattern and the functionals of our calculations agree, though I ran my calculations out only to time t=5.4.

The lift and drag coefficients in this study were calculated using formula (30). The results corresponding to this problem are plotted in Figures 26 and 27. The drag coefficient starts at zero, oscillates up and down giving an average of 0.49 after time t=5.2. Similarly the lift coefficient oscillates up and down. The average lift coefficient approaches the value 1.5 after time t=5.2.
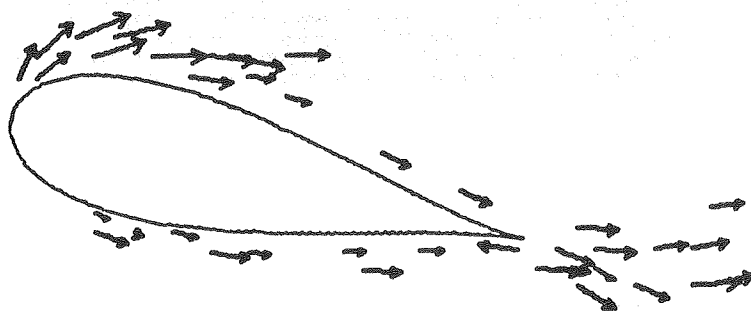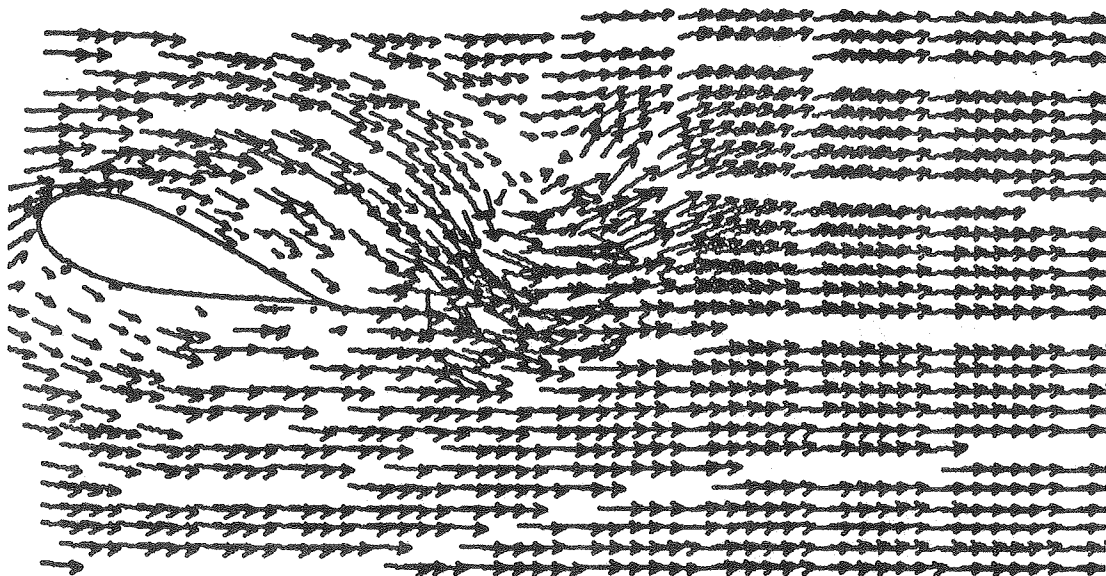
FIGURE 21   TIME T = 1
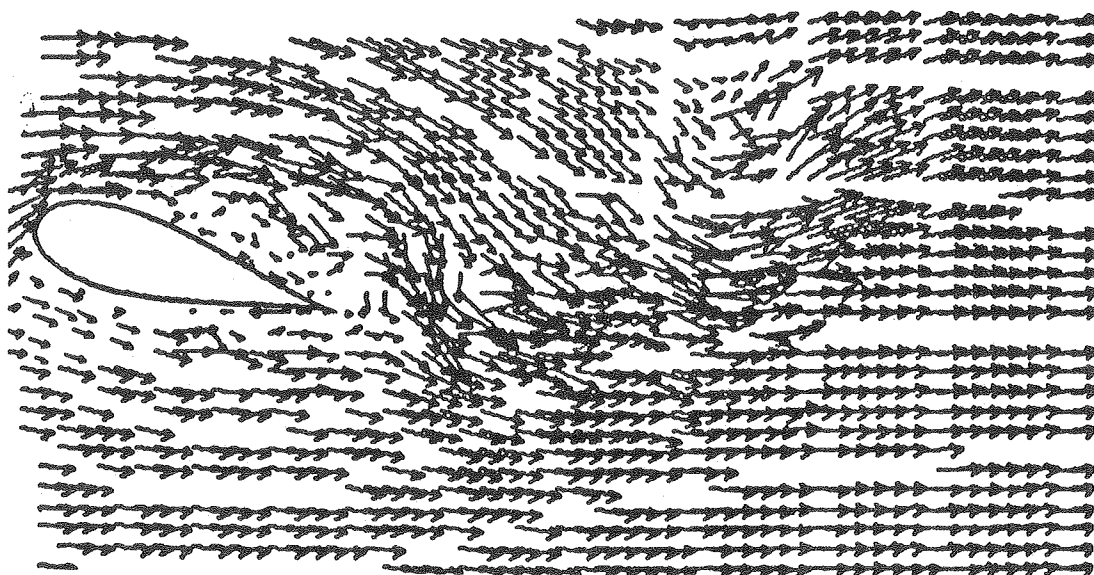
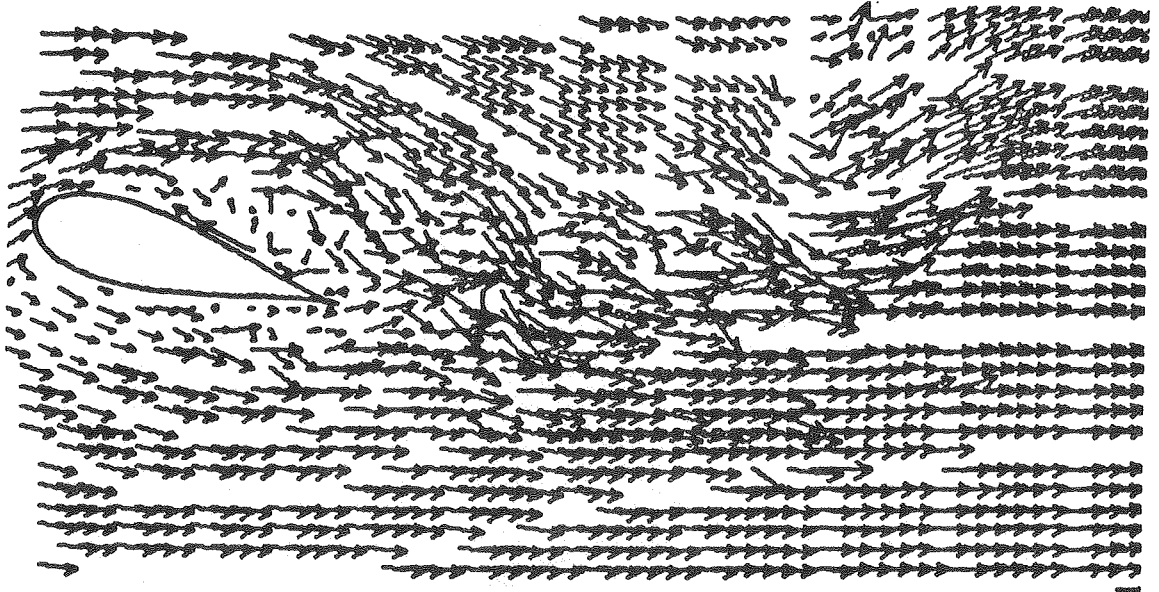FIGURE 22   TIME τ = 2

FIGURE 23   TIME τ = 4

FIGURE 24   TIME τ = 5

FIGURE 25   TIME τ = 5.4

FIGURE 26

drag coefficient
average drag

DRAG COEFFICIENT
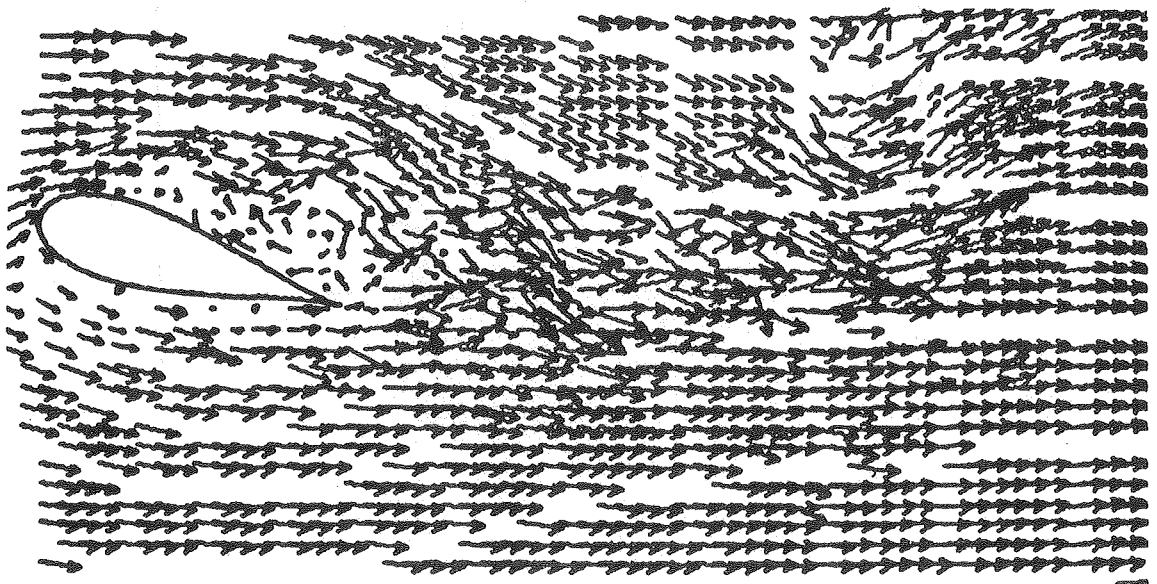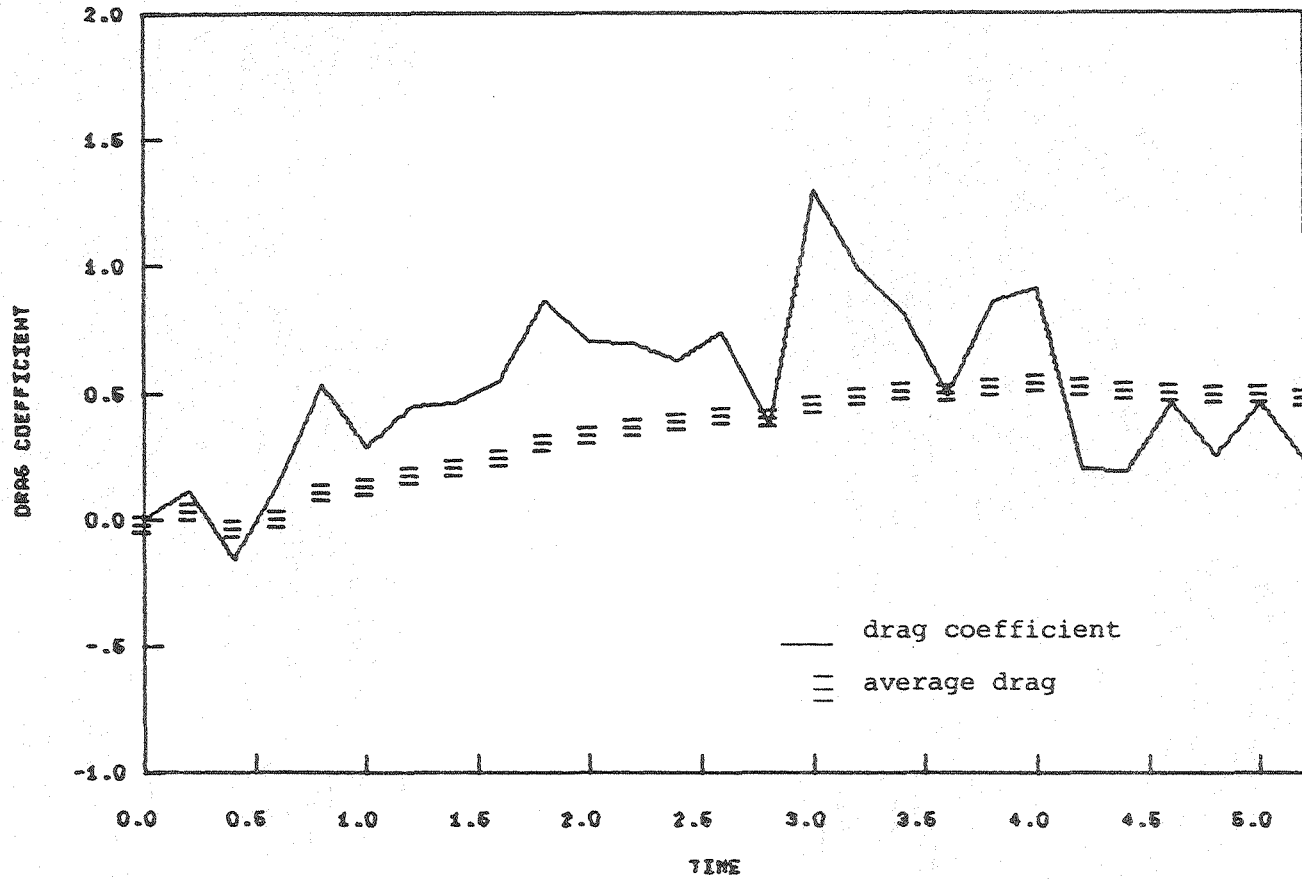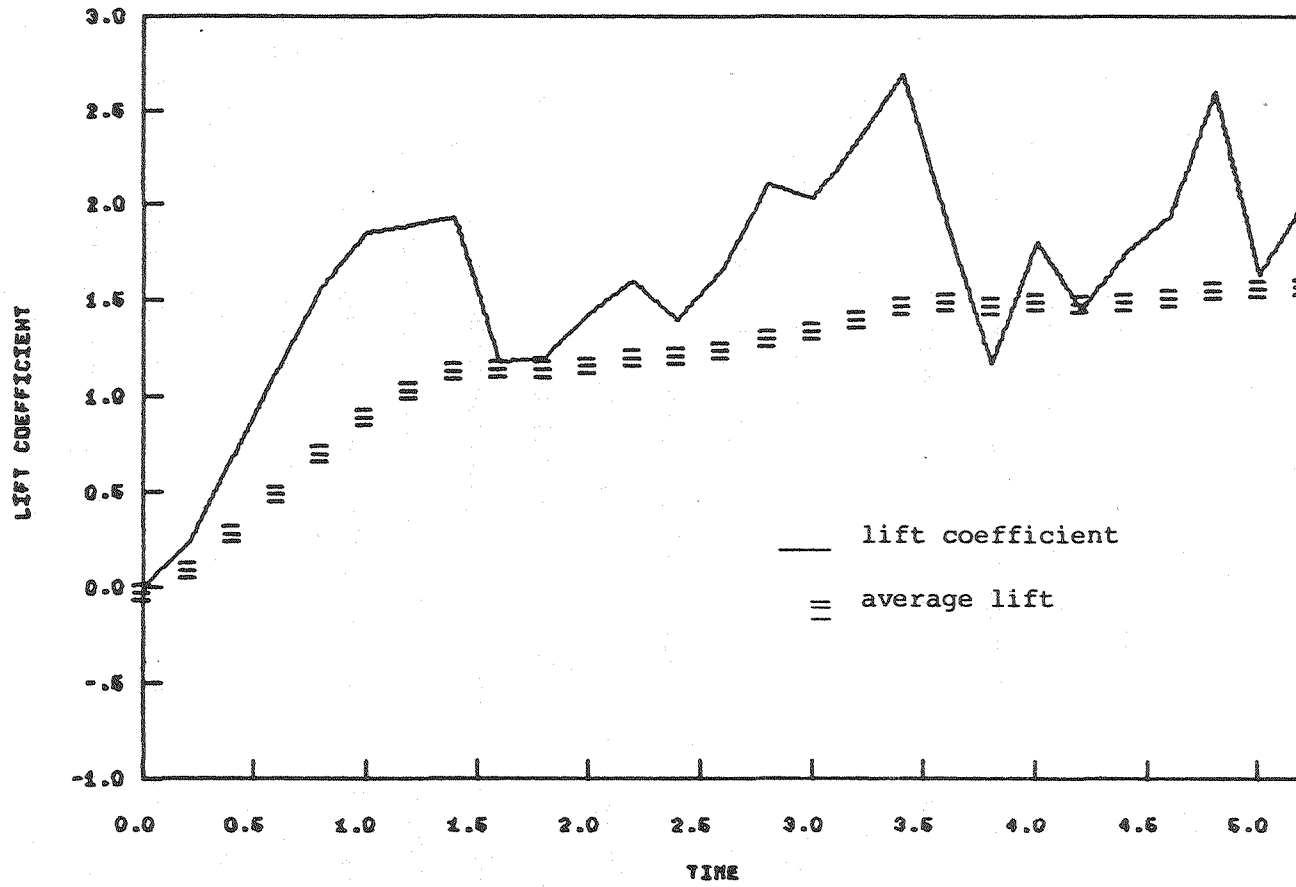
TIME

FIGURE 27

ii) The program was re-run with the Reynolds number changed to 5000. The flow realization corresponding to this run is plotted in Figures 28 to 31. The development of the flow is very close to the previous case with the bottom flow passing the tail end tangentially and the top flow separating close to the front of the airfoil. The circular eddies are seen quite clearly and are very strong by time t=5. Note that the behavior at the tail end of the airfoil is not singular. The flow passes this point tangentially and smoothly. The velocity magnitude of the flow in the vicinity of this point and in the wake of the airfoil is around 1.

Case III: $a = 0.25$ $\alpha = -\pi/6$ $R = 1000$

In this final numerical experiment, the airfoil is tilted at an angle of $-\pi/6$ radians. Again, the motion of the airfoil is started impulsively from rest in a fluid of density 1.

Initially the flow is potential and without circulation. The top point of separation does not coincide with the trailing edge. Soon after impulsive start, the top point of separation moves down and coincides with the rear of the airfoil. The flow in the first moments after starting actually shows a high velocity around the sharp trailing edge. However, a vortex of finite dimensions is formed at once.

The velocity above the airfoil is on the average larger than the velocity below the airfoil. Thus, uneven amounts of vorticity are being created, and different amounts of vorticity are shed from the top and from the bottom. As a result a circulation is produced. To satisfy the condition of conservation of circulation and the no-slip boundary condition, vorticity is created on the boundary.
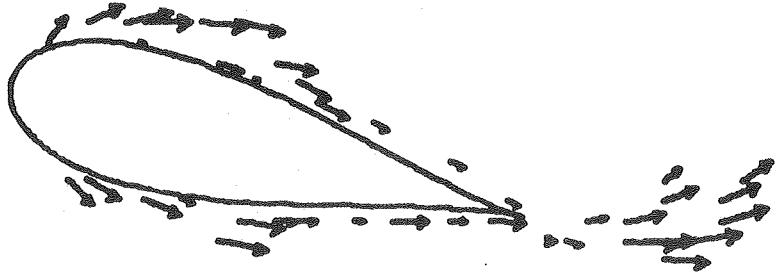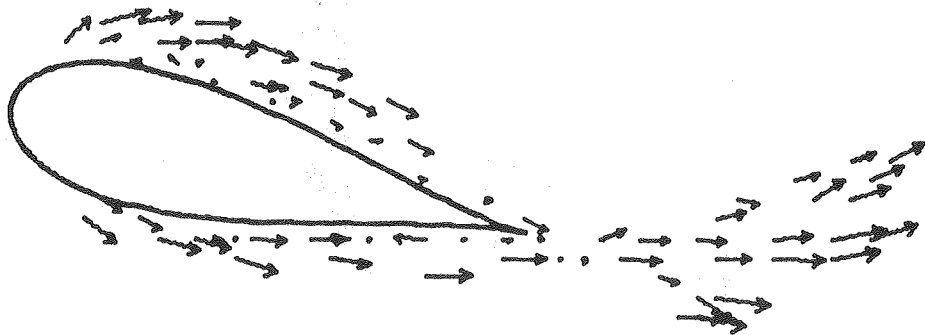
FIGURE 28   TIME T = 1
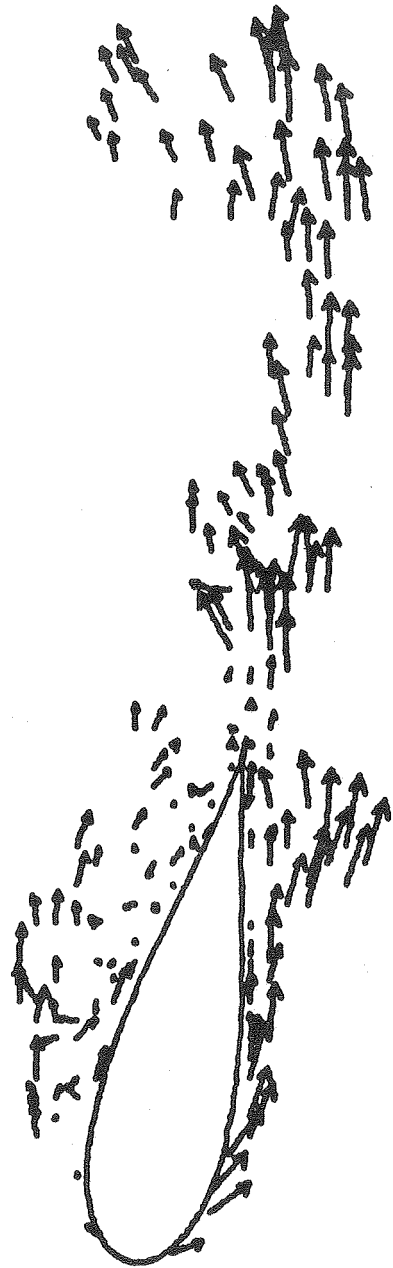
FIGURE 29   TIME T = 2

FIGURE 30   TIME τ = 4

Figure 31   Time т = 5

Almost immediately after impulsive start, the development of back-flow occurs in the boundary layer and the top point of separation moves up the airfoil toward the leading edge (see Figure 32). The deceleration of the fluid close to the body and the acceleration of the fluid above causes the flow in the boundary layer to curl up into circular patterns (see Figure 33). Downstream from the top separation point, the circular bubbles grow as they move down the airfoil. Eventually, they will be shed off the trailing edge. At time t=4, we see that the original circular bubble has moved downstream while a new circular bubble forms above the original one. The point of separation is now close to the leading edge of the airfoil (see Figure 35).

Following the development from time t=4 to time t=5, we see that the original bubble and the second bubble increase in size as they move farther down towards the tail end of the airfoil. Comparing this to Figure 2.19a, on page 37 of Schlichting [45], we see that our flow realization follows the development obtained from physical experiments (see Figures 36 and 37). For discussions on different numerical methods to solve flow past blunt bodies and airfoils, see Shen [47], Painkker and Lavan [40] and Orszag [39].
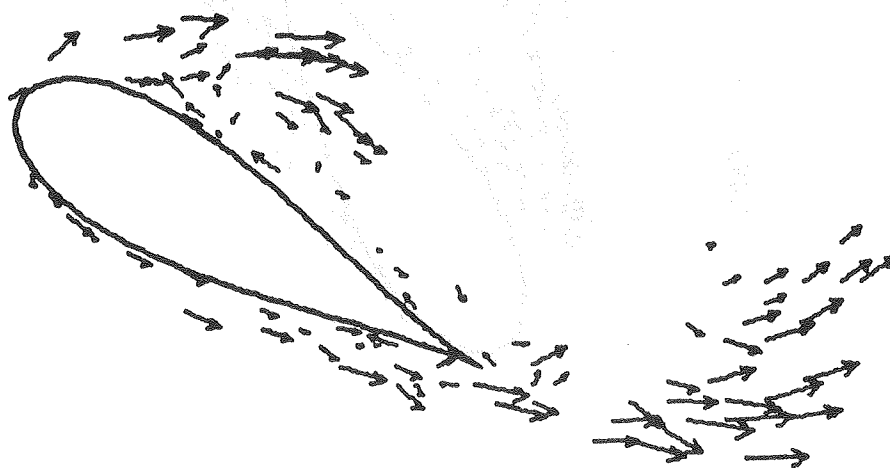
Figure 32   Time τ = 1

Figure 33   Time τ = 2

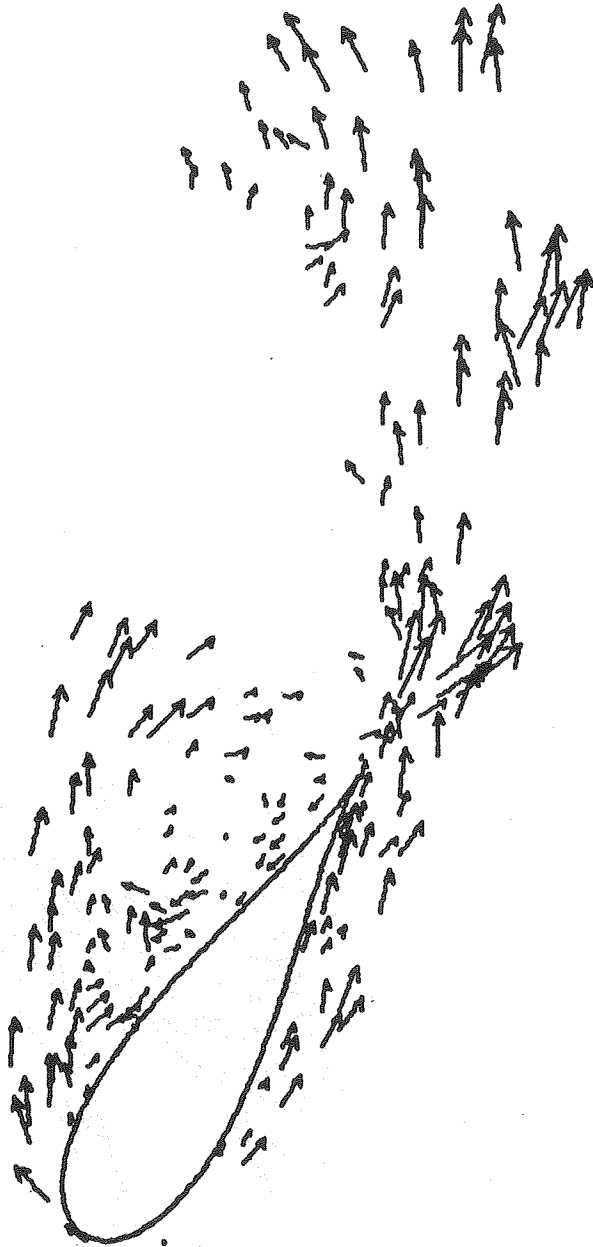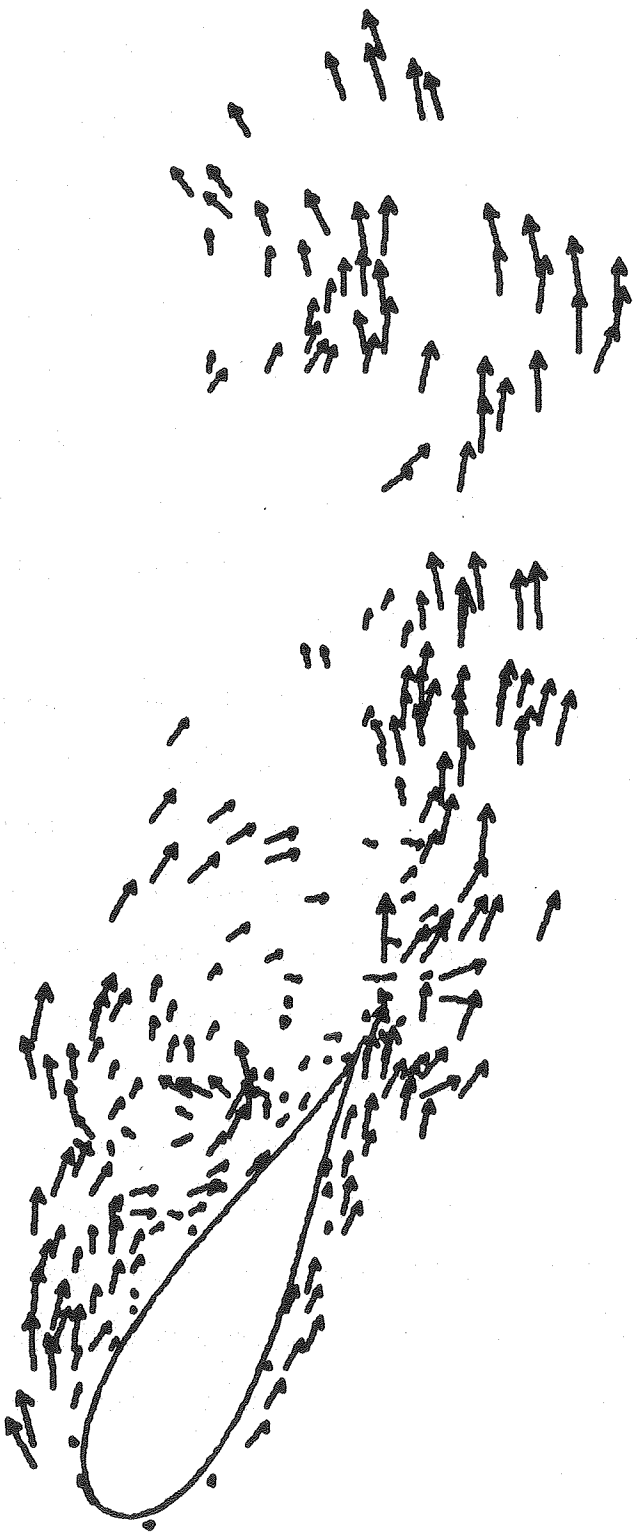Figure 34   Time τ = 3

Figure 35   Time $\tau = 4$

FIGURE 36   TIME T = 5

FIGURE 37   TIME T = 5.2

CONCLUSIONS

In the previous sections, we have introduced both the vortex-blobs and vortex-sheets methods. We then developed a hybrid algorithm by coupling these two methods. This hybrid algorithm was used to simulate flow past a circular cylinder, and flow past a Joukowski airfoil at varying angles of attack. We have seen that random-vortex methods for modeling the fluid flow past a circular cylinder yield results that are very accurate when compared to experimental data. Similarly, good results are obtained for flow past conformal transformation airfoils. This hybrid method is grid-free and can easily be adapted to give flow past objects of arbitrary shape.

Note that in our calculations no special assumption is made about the point of separation, no lower limit on the thickness of the boundary layer is imposed, there is no evidence of blow-up at the cusp end of the airfoil, and new computational elements are introduced only to satisfy the tangential boundary conditions. For a discussion of other vortex methods used for flow simulation, see A. Leonard [27], Kuwahara [24], and Sarpkaya and Schoaff [44].

There is hope that the algorithm presented in this paper can be expanded to study oscillating airfoils, three-dimensional flows and turbulence. Some existing results in this area, both numerical and experimental can be found in references [12], [29] to [33], and [52]. However, much more work in this area is required.

ACKNOWLEDGEMENTS

BIBLIOGRAPHY

[1] H. Ashley, and M. Landahl. Aerodynamics of Wing and Bodies, Addison-Wesley Publishing Company, Inc., Mass., 1975.

[2] L. Bairstow. Applied Aerodynamics, 2nd Edition, Longman's Green and Co., New York, 1939.

[3] G. K. Batchelor. An Introduction to Fluid Dynamics, Cambridge University Press, Cambridge, Great Britain, 1967.

[4] J. T. Beal and A. Majda. "Rates of Convergence for Viscous Splitting of the Navier-Stokes Equations," to appear in Math. Comp.

[5] A. Y. Cheer. "Program BOUNDL," LBL-6443 Suppl. Report, Lawrence Berkeley Laboratory, 1978.

[6] A. Y. Cheer. "A Study of Incompressible 2-D Vortex Flows Past a Circular Cylinder," LBL-9950, Lawrence Berkeley Laboratory, July 1979.

[7] A. Y. Cheer. "A Study of 2-D Vortex Flows Past Smooth Surfaces," Vortex Flows, presented at the Winter Annual Meeting of the American Society of Mechanical Engineers, Chicago, Illinois, November 16-20, (1980), pp. 141-154.

[8] A. J. Chorin and J. E. Marsden. A Mathematical Introduction to Fluid Mechanics, Springer-Verlag, New York Inc., 1979.

[9] A. J. Chorin. "Numerical Study of Slightly Viscous Flow," J.F.M., Vol. 57, (1973), pp. 785-796.

[10] A. J. Chorin. "Vortex Sheet Approximation of Boundary Layers," J of Comp. Physics, Vol. 27, (1978), pp. 428-442.

[11] A. J. Chorin, T. J. Hughes, M. F. McCracken and J. E. Marsden. "Product Formulas and Numerical Algorithms," Communications on Pure and Applied Math., Vol. 31, (1978), pp. 205-256.

[12] A. J. Chorin. "Vortex Models and Boundary Layer Instability," SIAM Jour. on Scientific Computing, Vol. 1, (1980), pp. 1-22.

[13] W. Frank. "Oscillation of Cylinders In or Below the Free Surface of Deep Fluids," Hydromechanics Laboratory Research and Development Report No. 2375, 1967.

[14] P. R. Garabedian. Partial Differential Equations, John Wiley and Sons Incs., New York, 1964.

[15] J. H. Gerrard. "The Mechanics of the Formation Region of Vortices Behind Bluff Bodies," JFM, Vol. 25, part 2, 1966, pp. 401-413.

[16] J. H. Gerrard. "A Disturbance-Sensitive Reynolds Number Range of the Flow Past a Circular Cylinder," JFM, Vol. 22, part 1, (1965), pp. 187-196.

[17] S. Goldstein. Modern Developments in Fluid Dynamics Vol. I and Vol. II, Dover Publications, Inc., New York, 1965.

[18] J. M. R. Graham. "The Forces on Sharpe-edged Cylinders in Oscillatory Flow at Low Keulegan-Carpenter Numbers." J.F.M. Vol. 97, part 1, (1980), pp. 331-346.

[19] O. H. Hald. "Convergence of Vortex Methods for Euler Equations: II," SIAM J. Numerical Analysis, Vol. 16, (1979), pp. 726-755.

[20] O. H. Hald. "Convergence of Random Methods for Reaction Diffusion Equation," to appear in SIAM J. Sci. Stat. Comput.

[21] O. H. Hald and V. M. DelPrete. "Convergence of Vortex Methods for Euler Equations," Mathematics of Computation, Vol. 32, (1978), pp. 791-809.

[22] J. M. Hammersley and D. C. Hamdsconb. Monte Carlo Methods, Methuen, London, 1964.

[23] I. Karasalo. Personal Communications, 1980.

[24] K. Kuwahara. "Study of Flow Past a Circular Cylinder by an Inviscid Model," J. of the Physical Society of Japan, Vol. 45, No. 1, (1978), pp. 292-297.

[25] H. Lamb. Hydrodynamics, Dover Publications, New York, 6th Ed., 1945.

[26] L. D. Landau and E. M. Lifshitz. Fluid Mechanics, Pergamon Press, New York, 1975.

[27] A. Leonard. "Vortex Methods for Flow Simulation," J. Comput. Physics, Vol. 37, (1980), pp. 289-335.

[28] C. C. Lin. "On the Motion of Vortices in Two Dimensions," University of Toronto Studies, Applied Math Series, No. 5, 1943.

[29] K. W. McAlister and L. W. Carr. "Water-Tunnel Experiments on an Oscillating Airfoil at Re = 21,000," NASA Technical Memorandum 78446, AMES Research Center, March 1978.

[30] W. J. McCroskey Notes on Unsteady Aerodynamics. Presented as part of the AGARD Lecture Series No. 94. Three-Dimensional and Unsteady Separation at High Reynolds Numbers, Von Karman Institute for Fluid Dynamics, Brussels, 20-24 February 1978.

[31] W. J. McCroskey. "Some Current Research in Unsteady Fluid Dynamics," J. of Fluids Engineering, Vol. 99, (March 1977), pp. 8-39.

[32] W. J. McCroskey, L. W. Carr, and K. W. McAlister. "Dynamic Stall Experiments on Oscillating Airfoils," AIAA Journal, Vol. 14, No. 1, (1976), pp. 57-63.

[33] U. Mehta. "Dynamic Stall of an Oscillating Airfoil," Presented at AGARD Fluid Dynamics Panel Symposium on Unsteady Aerodynamics, Ottawa, September 1977, Paper No. 23.

[34] U. Mehta and Z. Lavan. "Starting Vortex, Separation Bubbles and Stall: A Numerical Study of Laminar Unsteady Flow Around an Airfoil," J.F.M. Vol. 67, part 2, (1975), pp. 227-256.

[35] R. E. Meyer. Introduction to Mathematical Fluid Dynamics, John Wiley and Sons, Inc., 1971.

[36] Milne-Thomson. Theoretical Hydrodynamics, 3rd ed., MacMillian, New York, 1955.

[37] Milne-Thomson. Theoretical Aerodynamics, 4th ed., Dover Publications, Inc., New York, 1966.

[38] A. N. Nahavandi and S. S. Chen. "A Review on Fluid Forces on Circular Cylinders in Cross Flow," Argonne National Laboratory Technical Memorandum, January 1979.

[39] S. A. Orszag and M. Israeli. "Numerical Simulation of Viscous Incompressible Flows," Ann. Rev. Fluid Mech. (1974), pp. 281-318.

[40] P. K. G. Painkker and Z. Lavan. "Flow Past Impulsively Started Bodies Using Green's Functions," J. of Comp. Physics Vol. 18, (1975), pp. 46-65.

[41] L. Prandtl and O. G. Tietjens. Applied Hydro and Aeromechanics, Dover Publications, New York 1957.

[42] A. Robinson. Wing Theory, Cambridge University Press, Cambridge, 1956.

[43] R. Rogallo. Personal Communication, 1979.

[44] T. Sarpkaya and R. L. Schoaff. "Inviscid Model of Two-Dimensional Vortex Shedding by a Circular Cylinder," AIAA Journal, Vol. 17, No. 11, (November 1979), pp. 1193-1200.

[45] H. Schlichting. Boundary Layer Theory, 7th edition, McGraw-Hill, New York, 1979.

[46] L. A. Segel. Mathematics Applied to Continuum Mechanics, MacMillian Publishing Co., Inc., New York, 1977.

[47] S. Shen. "Finite-Element Method in Fluid Mechanics," Ann. Rev. Fluid Mech., Vol. 9, (1977), pp. 421-45.

[48] D. G. Shepherd. Elements of Fluid Mechanics, Harcourt, Brace and World, New York, 1965.

[49] F. H. Sighard. Fluid Dynamics Drag, Published by Author, 1958.

[50] I. Tani. "History of Boundary Layer Theory," Ann. Rev. Fluid Mech. Vol. 9, (1977), pp. 87-111.

[51] D. J. Tritton. "A Note on Vortex Streets Behind Circular Cylinders at Low Reynold's Numbers," J.F.M. Vol. 45, part 1, (1971), pp. 203-208.

[52] K. C. Wang. "Boundary Layer Over a Blunt Body at Low Incidence with Circumferential Reversed Flow," J.F.M. Vol. 72, part 1, (1975), pp. 49-65.

[53] W. C. Webster. "Computation of Hydrodynamic Forces Induced by General Vibration of Cylinders," J. of Ship Research, Vol. 23, (1967), pp. 9-19.

[54] F. M. White. Viscous Fluid Flow, McGraw Hill, New York, 1974.

[55] J. C. Williams, III. "Incompressible Boundary Layer Separation," Ann. Rev. Fluid Mech. Vol. 9, (1977), pp. 113-44.

[56] J. C. Wu, S. Sampath and N. L. Sankar. "A Numerical Study of Viscous Flows around Airfoils," Presented at AGARD Fluid Dynamics Panel Symposium on Unsteady Aerodynamics, Ottawa, Canada, September 1977.